White Rose Research Online

eprints@whiterose.ac.uk
https://eprints.whiterose.ac.uk
Universities of Leeds, Sheffield and York

Deposited via The University of York.

White Rose Research Online URL for this paper:
https://eprints.whiterose.ac.uk/id/eprint/155084/

Version: Published Version

**Article:**
Martínez-Martínez, Antonio J., Tegner, Bengt E., McKay, Alasdair I. et al. (2018) Modulation of σ-Alkane Interactions in [Rh(L2)(alkane)]+ Solid-State Molecular Organometallic (SMOM) Systems by Variation of the Chelating Phosphine and Alkane: Access to η2,η2-σ-Alkane Rh(I), η1-σ-Alkane Rh(III) Complexes, and Alkane Encapsulation. Journal of the American Chemical Society. pp. 14958-14970. ISSN: 1520-5126

https://doi.org/10.1021/jacs.8b09364

**Reuse**
This article is distributed under the terms of the Creative Commons Attribution (CC BY) licence. This licence allows you to distribute, remix, tweak, and build upon the work, even commercially, as long as you credit the authors for the original work. More information and the full terms of the licence here: https://creativecommons.org/licenses/

**Takedown**
If you consider content in White Rose Research Online to be in breach of UK law, please notify us by emailing eprints@whiterose.ac.uk including the URL of the record and the reason for the withdrawal request.

UNIVERSITY OF LEEDS
University of Sheffield
UNIVERSITY of York

This is an open access article published under a Creative Commons Attribution (CC-BY) License, which permits unrestricted use, distribution and reproduction in any medium, provided the author and source are cited.

JACS JOURNAL OF THE AMERICAN CHEMICAL SOCIETY

Article

Cite This: J. Am. Chem. Soc. 2018, 140, 14958−14970

pubs.acs.org/JACS

# Modulation of σ-Alkane Interactions in [Rh(L$_2$)(alkane)]$^+$ Solid-State Molecular Organometallic (SMOM) Systems by Variation of the Chelating Phosphine and Alkane: Access to $\eta^2,\eta^2$-σ-Alkane Rh(I), $\eta^1$-σ-Alkane Rh(III) Complexes, and Alkane Encapsulation

Antonio J. Martínez-Martínez,[†] Bengt E. Tegner,[‡] Alasdair I. McKay,[†] Alexander J. Bukvic,[†] Nicholas H. Rees,[†] Graham J. Tizzard,[§] Simon J. Coles,[§] Mark R. Warren,[∥] Stuart A. Macgregor,*[,‡] and Andrew S. Weller*[,†]

[†]Chemistry Research Laboratories, University of Oxford, Oxford OX1 3TA, United Kingdom

[‡]Institute of Chemical Sciences, Heriot-Watt University, Edinburgh EH14 4AS, United Kingdom

[§]UK National Crystallography Service, Chemistry, Faculty of Natural and Environmental Sciences, University of Southampton, Southampton SO17 1BJ, United Kingdom

[∥]Harwell Science and Innovation Campus, Diamond Light Source Ltd., Didcot OX11 0DE, United Kingdom

Supporting Information

**ABSTRACT:** Solid/gas single-crystal to single-crystal (SC−SC) hydrogenation of appropriate diene precursors forms the corresponding σ-alkane complexes [Rh(Cy$_2$P(CH$_2$)$_n$PCy$_2$)(L)][BAr$^F_4$] ($n$ = 3, 4) and [RhH(Cy$_2$P(CH$_2$)$_2$(CH)(CH$_2$)$_2$PCy$_2$)(L)][BAr$^F_4$] ($n$ = 5, L = norbornane, NBA; cyclooctane, COA). Their structures, as determined by single-crystal X-ray diffraction, have cations exhibiting Rh···H−C σ-interactions which are modulated by both the chelating ligand and the identity of the alkane, while all sit in an octahedral anion microenvironment. These range from chelating $\eta^2,\eta^2$ Rh···H−C (e.g., [Rh(Cy$_2$P(CH$_2$)$_n$PCy$_2$)($\eta^2\eta^2$-NBA)][BAr$^F_4$], $n$ = 3 and 4), through to more weakly bound $\eta^1$ Rh···H−C in which C−H activation of the chelate backbone has also occurred (e.g., [RhH(Cy$_2$P(CH$_2$)$_2$(CH)(CH$_2$)$_2$PCy$_2$)($\eta^1$-COA)][BAr$^F_4$]) and ultimately to systems where the alkane is not ligated with the metal center, but sits encapsulated in the supporting anion microenvironment, [Rh(Cy$_2$P(CH$_2$)$_3$PCy$_2$)][COA⊂BAr$^F_4$], in which the metal center instead forms two intramolecular agostic $\eta^1$ Rh···H−C interactions with the phosphine cyclohexyl groups. $CH_2Cl_2$ adducts formed by displacement of the $\eta^1$-alkanes in solution ($n$ = 5; L = NBA, COA), [RhH(Cy$_2$P(CH$_2$)$_2$(CH)(CH$_2$)$_2$PCy$_2$)($\kappa^1$-ClCH$_2$Cl)][BAr$^F_4$], are characterized crystallographically. Analyses via periodic DFT, QTAIM, NBO, and NCI calculations, alongside variable temperature solid-state NMR spectroscopy, provide snapshots marking the onset of Rh···alkane interactions along a C−H activation trajectory. These are negligible in [Rh(Cy$_2$P(CH$_2$)$_3$PCy$_2$)][COA⊂BAr$^F_4$]; in [RhH(Cy$_2$P(CH$_2$)$_2$(CH)(CH$_2$)$_2$PCy$_2$)($\eta^1$-COA)][BAr$^F_4$], $\sigma_{C-H}$ → Rh σ-donation is supported by Rh → $\sigma^*_{C-H}$ "pregostic" donation, and in [Rh(Cy$_2$P(CH$_2$)$_n$PCy$_2$)($\eta^2\eta^2$-NBA)][BAr$^F_4$] ($n$ = 2−4), σ-donation dominates, supported by classical Rh(dπ) → $\sigma^*_{C-H}$ π-back-donation. Dispersive interactions with the [BAr$^F_4$]$^-$ anions and Cy substituents further stabilize the alkanes within the binding pocket.

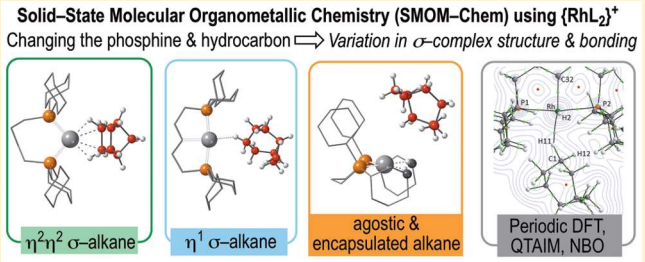


## 1. INTRODUCTION

The ability to tune the local environment around a metal center by variation of supporting ligands is an important concept widely used in homogeneous organometallic synthesis and catalysis.[1,2] A well-documented example of this comes from bidentate phosphine ML$_2$-type complexes,[3,4] as by altering the L−M−L bite-angle and substitution at phosphine the resulting steric (e.g., the solid-cone angle, Θ[5]), or electronic (e.g., oxidation state[6] or degree of bond activation[7]), changes ultimately can provide the ability to control structure, speciation, and, through the energetics of elementary reaction steps in catalysis, activity and selectivity. Figure 1A.

Extending such concepts to heterogeneous systems is difficult given the resulting challenges associated with precisely defining single-site active centers and their extended coordination environments.[8] While chelating phosphine complexes supported by metal−organic frameworks,[9] porous coordination polymers,[10] nanoparticles,[11] mesoporous hosts,[12] and silica surfaces[13] have

Received: August 30, 2018
Published: October 10, 2018

Downloaded via UNIV OF YORK on January 3, 2020 at 12:16:51 (UTC).
See https://pubs.acs.org/sharingguidelines for options on how to legitimately share published articles.

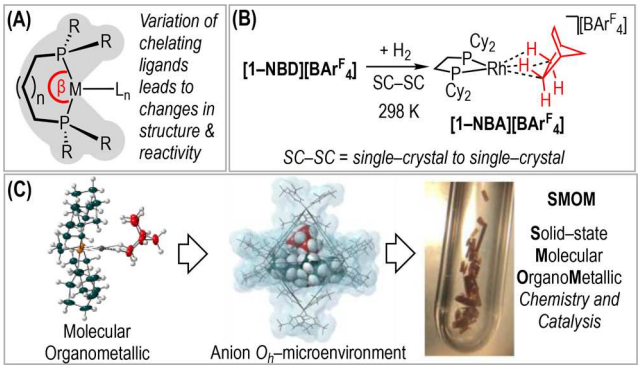


**Figure 1.** (A) Control of local environment in $\{ML_2\}$ complexes: bite-angle = $\beta$. (B) Synthesis of the $\sigma$-alkane complex [**1-NBA**][**BAr$^F_4$**]: NBD = norbornadiene. (C) The SMOM concept.

been reported, the role of the chelating ligand in determining structure and reactivity is less well-developed. Nevertheless, precise control of well-defined, and reactive, metal centers in heterogeneous systems could lead to enhanced activity and selectivity in catalysis, as frequently demonstrated in homogeneous processes.[1,4]

We have recently shown that single-crystal to single-crystal (SC−SC) solid/gas reactions between $H_2$ and the appropriate $[RhL_2(diene)]^+$ precursors form well-defined but reactive $\sigma$-alkane[14−16] complexes directly in the solid-state, e.g., $[Rh(Cy_2P(CH_2)_2PCy_2)(\eta^2\eta^2\text{-NBA})][BAr^F_4]$, [**1-NBA**][**BAr$^F_4$**] (NBA = norbornane, $Ar^F$ = 3,5-$(CF_3)_2C_6H_3$), Figure 1B).[17−20] Such $\sigma$-complexes contain 3-center 2-electron (3c−2e) Rh···H−C bonds[21,22] and are of general interest from the fundamental challenges presented by their synthesis and characterization,[14,15] as well as their central role as intermediates in C−H activation processes.[23−26] When prepared in this way, these $\sigma$-alkane complexes show remarkable relative stability compared with species prepared by solution routes; the latter are generally characterized in situ using NMR spectroscopy, on a small scale (2−20 mg) at very low temperature, and have limited lifetimes even under these relatively constrained conditions.[27−31]

This stability in the solid-state originates from the $[BAr^F_4]^-$ anions providing a robust, octahedral, crystalline microenvironment[32] that allows for isolation, characterization, and onward reactivity of the encapsulated organometallic cation to be studied in detail (Figure 1C).[26,33] These so-called[33] solid-state molecular organometallic (SMOM) systems are related to supported organometallic catalysts (SOMC),[13] single-site heterogeneous catalysts (SSHC),[34] and MOF-functionalized organometallics[9,35−37] but, in contrast to these, are not supported by a platform material. Moreover, SMOM systems have the desirable properties of being readily studied at the molecular-level by single-crystal X-ray diffraction, solid-state NMR (SSNMR) spectroscopy, and computational techniques such as periodic DFT.

We now report that systematic variation of the P−Rh−P bite-angle coupled with the identity of the diene in SMOM systems based upon precursors $[Rh(Cy_2P(CH_2)_nPCy_2)(diene)][BAr^F_4]$ ($n$ = 3 to 5, diene = norbornadiene, NBD, or 1,5-cyclooctadiene, COD, Scheme 1) results in significant changes in structure and reactivity on addition of $H_2$ in SC−SC reactions. This results in crystallographically characterized $\sigma$-alkane complexes that show markedly different degrees of Rh···H−C interaction in response to the changes in *both* phosphine and the precursor diene, while they are stabilized in the microenvironment provided by the octahedral arrangement of $[BAr^F_4]^-$ anions: these range from

**Scheme 1. Precursor Diene Complexes Used in This Study and SC−SC SMOM Synthesis of $\sigma$-Complexes**

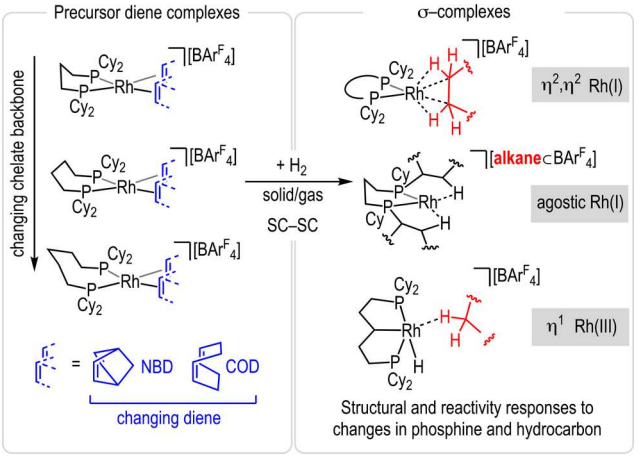


chelating $\eta^2,\eta^2$ Rh···H−C, through to more weakly bound $\eta^1$ Rh··H−C and ultimately to systems where the alkane is not ligated with the metal center but sits encapsulated in the anion framework.

## 2. RESULTS AND DISCUSSION

**2.1. Precursor Diene Complexes.** Precursor complexes of the general formula $[Rh(Cy_2P(CH_2)_nPCy_2)(diene)][BAr^F_4]$ (diene = NBD or COD) were prepared in which the phosphine and diene are systematically varied: $n$ = 3, [**2-diene**][**BAr$^F_4$**]; $n$ = 4, [**3-diene**][**BAr$^F_4$**]; $n$ = 5, [**4-diene**][**BAr$^F_4$**] (Scheme 2). These

**Scheme 2. (A) Synthesis of Diene Precursors and (B) Representative P−Rh−P Bite-Angles ($\beta$) Taken from Diene Structures[17,39]**

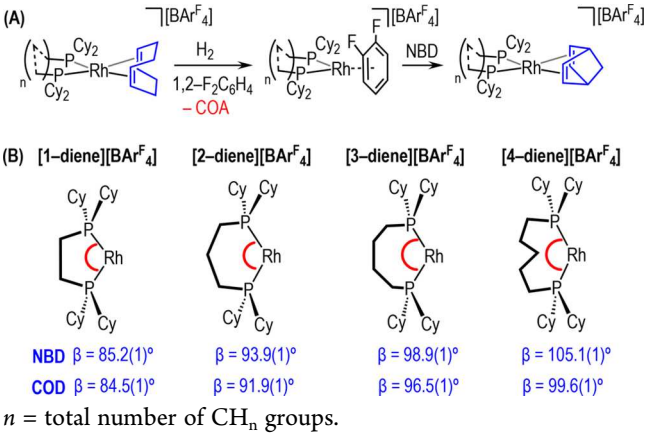


$n$ = total number of $CH_n$ groups.

are conveniently prepared by reaction of $[Rh(COD)_2][BAr^F_4]$ with $Cy_2P(CH_2)_nPCy_2$ to give $[Rh(Cy_2P(CH_2)_nPCy_2)(COD)][BAr^F_4]$, followed by addition of $H_2$/1,2-$F_2C_6H_4$/NBD to give $[Rh(Cy_2P(CH_2)_nPCy_2)(NBD)][BAr^F_4]$ via in situ formation of difluorobenzene-bound[38] intermediates $[Rh(Cy_2P(CH_2)_nPCy_2)(1,2\text{-}F_2C_6H_4)][BAr^F_4]$. Both COD and NBD precursors were isolated in good (~80%) yield after recrystallization from $CH_2Cl_2$/pentane. Complexes [**1-diene**][**BAr$^F_4$**] ($n$ = 2) have previously been reported.[18]

These precursor complexes have been characterized by solution NMR spectroscopy and single-crystal X-ray diffraction, the latter which shows an $O_h$ arrangement of $[BAr^F_4]^-$ anions


DOI: 10.1021/jacs.8b09364
J. Am. Chem. Soc. 2018, 140, 14958−14970

surrounding the organometallic cations, as observed for [**1-NBA**][**BAr$^F_4$**][18] and related complexes.[17,20] The Supporting Information details their structures. For the NBD precursors, this homologous series allows for the bite-angle ($\beta$) of the various diphosphines in this environment to be compared. Unsurprisingly,[4] $\beta$ becomes progressively larger with an increasing number of methylene units in the chelate backbone (Scheme 2B). The same trend, albeit interestingly with slightly smaller $\beta$-angles, is apparent for the COD precursors. With these complexes in hand a systematic study of solid/gas hydrogenation was undertaken.

**2.2. Hydrogenation of {Rh(Cy$_2$P(CH$_2$)$_2$PCy$_2$)}$^+$/COD.** As previously reported,[18] hydrogenation of [**1-NBD**][**BAr$^F_4$**] gives [**1-NBA**][**BAr$^F_4$**] in a rapid (less than 10 min) SC−SC transformation (see Figure 1B). Here, use of [**1-COD**][**BAr$^F_4$**] results a slower[40,41] reaction with $H_2$ (3 h) and loss of crystallinity. Dissolving the resulting solid in $CD_2Cl_2$ afforded the previously reported zwitterion [Rh(Cy$_2$P(CH$_2$)$_2$PCy$_2$){($\eta$-C$_6$H$_3$(CF$_3$)$_2$)BAr$^F_3$}], [**1-BAr$^F_4$**], and free COA.[18]

**2.3. {Rh(Cy$_2$P(CH$_2$)$_3$PCy$_2$)}$^+$/NBA: An $\eta^2$,$\eta^2$ $\sigma$-Alkane Complex.** Addition of $H_2$ (1 bar, 298 K) to single-crystals of [Rh(Cy$_2$P(CH$_2$)$_3$PCy$_2$)(NBD)][BAr$^F_4$], [**2-NBD**][**BAr$^F_4$**], resulted in the rapid (~5 min) formation of the $\sigma$-alkane complex [Rh(Cy$_2$P(CH$_2$)$_3$PCy$_2$)($\eta^2$,$\eta^2$-NBA)][BAr$^F_4$], [**2-NBA**][**BAr$^F_4$**], in an SC−SC transformation, as shown by single-crystal X-ray diffraction (Figure 2) and $^{31}$P{$^1$H}/$^{13}$C{$^1$H}

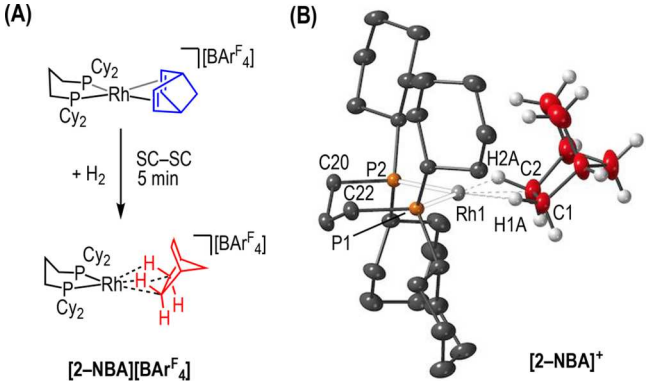


**Figure 2.** (A) Synthesis of [**2-NBA**][**BAr$^F_4$**]. (B) Cation of [**2-NBA**][**BAr$^F_4$**]. 50% displacement ellipsoids. Selected bond lengths (Å) and angles (deg): Rh1···C1 2.408(2); Rh1···C2, 2.402(2); C1−C2, 1.554(3); Rh1−P1, 2.2065(4); Rh1−P2, 2.2049(4); P1−Rh1−P2, 93.91(2); Rh1−H1A−C1, 105.1(2); Rh1−H2A−C2, 106.0(2); ∠P1P2Rh/Rh1C1C2, 5.15(7).

SSNMR spectroscopies. The octahedral arrangement of [BAr$^F_4$]$^-$ anions is retained in [**2-NBA**][**BAr$^F_4$**][39] while the central cation is pseudo square-planar, with the {RhL$_2$}$^+$ fragment bound to the alkane NBA through two *endo* Rh···H−C $\sigma$ interactions showing relatively short Rh···C distances [Rh···C 2.408(2)/2.402(2) Å] and rather acute ∠RhHC, e.g., Rh1−H1A−C1 105.1(2)°. These H atoms were located and freely refined. These data suggest an $\eta^2$,$\eta^2$ chelating Rh···H−C motif,[14,42] as corroborated by computational studies (see later). Despite the P−Rh−P bite-angle increasing compared with [**1-NBA**][**BAr$^F_4$**][18] (e.g., Scheme 2B), the Rh···C distances are not different within error [cf. 2.389(3)/2.400(3) Å] and the structures are very similar, suggesting that the NBA ligand fits comfortably into the ligand pocket defined by the Cy groups. This similarity is not strongly influenced by the anion microenvironment as evidenced by calculations on isolated cations (Section 2.7 and Supporting Information). In the solid-state, there are a number of weak C−H···F interactions between the NBA ligand and the [BAr$^F_4$]$^-$ anion, Figure S73.

The $^{31}$P{$^1$H} SSNMR spectrum of [**2-NBA**][**BAr$^F_4$**] shows two relatively sharp environments at $\delta$ = 50.6, 51.6 [$J$(RhP) = ~170 Hz], while the $^{13}$C{$^1$H} NMR spectrum is featureless between $\delta$ 110 and 50, demonstrating hydrogenation of the NBD. A $^1$H/$^{13}$C frequency switched Lee−Goldburg (FSLG) HETCOR experiment at 298 K, which has been used to characterize E−H···M interactions in the solid-state (E = Si, C),[18,26,43] shows two strong correlations between $\delta$($^{13}$C) = ~26 and $\delta$($^1$H) = −2 which are consistent with the crystallographically inequivalent Rh···H−C interactions observed in the solid-state (Figure S13). An additional correlation [$\delta$($^{13}$C) 42/$\delta$($^1$H) = −0.6][44] is assigned to the CH$_2$ bridge on the norbornane, which is affected by [BAr$^F_4$] ring-current effects as described for [**1-NBA**][**BAr$^F_4$**] and related complexes.[18,19,26]

Dissolving crystalline material of [**2-NBA**][**BAr$^F_4$**] in $CD_2Cl_2$ at 183 K results in free NBA being observed by $^1$H NMR spectroscopy and a $^{31}$P{$^1$H} NMR spectrum that is suggestive of a solvent-coordinated complex, [Rh(Cy$_2$P(CH$_2$)$_3$PCy$_2$)-(ClCH$_2$Cl)$_n$][BAr$^F_4$], $\delta$ 47.4 [$J$(RhP) = 198 Hz], similar to that reported for [Rh($^i$Pr$_2$P(CH$_2$)$_3$P$^i$Pr$_2$)(ClCH$_2$CH$_2$Cl)]-[BAr$^F_4$].[18] On warming, decomposition occurs via C−Cl activation to give a mixture of partially soluble chloride-bridged hydride dimers, e.g., [Rh(Cy$_2$P(CH$_2$)$_3$PCy$_2$)H($\mu$-Cl)]$_2$[BAr$^F_4$]$_2$, that precipitate from solution and are best identified by ESI-MS. The formation of the [BAr$^F_4$]$^-$-coordinated zwitterion was not observed,[45] in contrast to [**1-NBA**][**BAr$^F_4$**] that forms [**1-BAr$^F_4$**] in $CD_2Cl_2$.[18] We suggest this is a consequence of the increased steric profile of the chelating phosphine Cy$_2$P(CH$_2$)$_3$PCy$_2$ versus Cy$_2$P(CH$_2$)$_2$PCy$_2$, disfavoring coordination of the, local to the metal center, planar and bulky [BAr$^F_4$]$^-$ anion, coupled with the wider bite-angle phosphines encouraging oxidative addition at Rh(I).[6]

**2.4. {Rh(Cy$_2$P(CH$_2$)$_3$PCy$_2$)}$^+$/COA: A 12-Electron Rh(I) Complex Supported by Agostic Interactions with an Encapsulated Nonbonding Alkane.** Exposing single crystals of [**2-COD**][**BAr$^F_4$**] to $H_2$ for 3 h results in, slower,[40,41] SC−SC hydrogenation and expulsion of cyclooctane (COA) from the metal center to form formally 12-electron "naked"[46,47] [Rh(Cy$_2$P-(CH$_2$)$_3$PCy$_2$)]$^+$, [**2**]$^+$. Remarkably, the free alkane is retained inside the anion octahedral cavity to give [Rh(Cy$_2$P(CH$_2$)$_3$-PCy$_2$)][COA⊂BAr$^F_4$], [**2**][**COA⊂BAr$^F_4$**], Scheme 3.

**Scheme 3. Synthesis of [2][COA⊂BAr$^F_4$]**

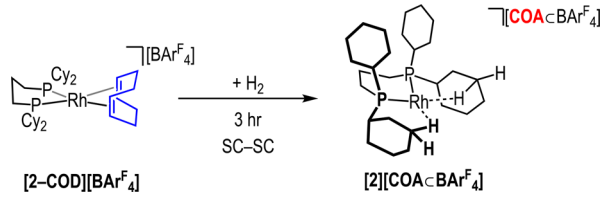


The solid-state structure of the cation [**2**]$^+$ (Figure 3A) shows two $\delta$-agostic[48−50] Rh···H−C interactions from the cyclohexyl rings [Rh···C3 2.91(1) Å, Rh···C9 2.87(1) Å] that form in response to the unsaturation now at the Rh(I) metal center. The Rh1−P1−C1 angle reflects this, for example, being more acute [108.9(3)°] than Rh1−P1−C13 [119.8(3)°]. The Rh center also moves toward the C−H bonds involved in these agostic interactions, as shown by the angle between the planes ∠P1P2C25C27/Rh1P1P2 = 42.6(2)° (Figure 3B).


DOI: 10.1021/jacs.8b09364
J. Am. Chem. Soc. 2018, 140, 14958−14970

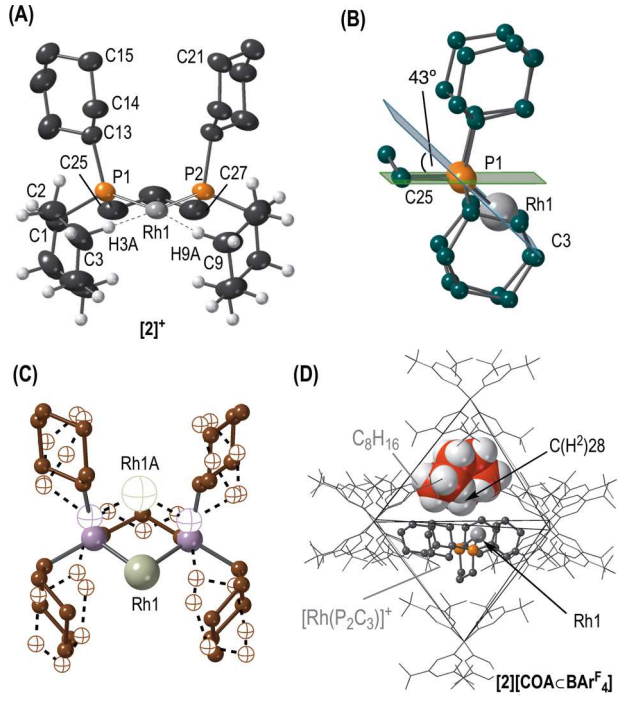


**Figure 3.** (A) Cation of [**2**][**COA⊂BAr$^F_4$**]. 50% displacement ellipsoids, only the major disordered component shown. Selected bond lengths (Å) and angles (deg): Rh1···C3, 2.912(10); Rh1···C9, 2.873(10); Rh1−P1, 2.171(2); Rh1−P2, 2.166(2); P1−Rh1−P2, 91.21(8); ∠P1P2C25C27/Rh1P1P2, 42.6(2). (B) Displacement of the Rh center in [**2**]$^+$ toward the agostic C−H bonds in the major disordered component. (C) Ball and stick representation of the two disordered components in [**2**]$^+$. (D) Packing diagram of [**2**][**COA⊂BAr$^F_4$**] showing the $O_h$ arrangement of [BAr$^F_4$]$^-$, COA (C = red) shown at van der Waals radii, and only one disordered component shown, Rh1···C28, 3.74(1) Å.

The relatively long Rh···C distances, coupled with more open ∠RhHC angles, e.g., Rh1−H9A−C9 147.9(6)°, albeit with the hydrogens placed in calculated positions, suggests an $\eta^1$ Rh···H−C bonding motif for the agostic interactions, a view supported by calculations (see Section 2.7). This movement of the metal center keeps the phosphine ligand in essentially the same environment in the anion cavity and maximizes the Rh···H−C agostic interactions, with two cyclohexyl groups also enfolding the metal center.[51] It also retains the square planar geometry around Rh, with angles around the metal center = 360°. A minor, disordered, agostomeric[52] component is also present (∼10%) in which the Rh center swings up to interact with the chemically equivalent C15−H and C21−H bonds (Figure 3C). The Rh−P distances in the major component [2.166(2) and 2.171(2) Å] are ∼0.04 Å shorter than in [**2-NBA**][**BAr$^F_4$**]. Whether this reflects a weaker *trans*-influence of the bis-agostic Rh···H−C interactions in [**2**][**COA⊂BAr$^F_4$**] compared with the intermolecular interactions in [**2-NBA**][**BAr$^F_4$**], or is a consequence of the metal's unusual disposition, is not clear. Although formally 2-coordinate group 9 complexes are known,[53,54] albeit rare, as far as we are aware the cation in [**2**][**COA⊂BAr$^F_4$**] is the first example reported with a chelating phosphine.

The expelled alkane, COA, sits encapsulated[55,56] within the anion framework (Figure 3D), essentially equally disordered between two boat−chair conformations.[57] The closest Rh···C distance is 3.74(1) Å (C28), approaching the Rh center above the square plane, suggesting no significant, and at best very weak, interaction with the metal center. This distance is similar to that measured in [U(ArO)$_3$(neo-hexane)] [3.731(8) Å], albeit U versus Rh] where a bonding interaction was suggested,[58] although studies on related uranium complexes suggest that such as distance reflects a nonbonding interaction.[59]

In the 158 K $^{31}$P{$^1$H} SSNMR spectrum of [**2**][**COA⊂BAr$^F_4$**] only two broad (fwhm ∼400 Hz) environments are observed at $\delta$ 51.3 and $\delta$ 48.1 in an approximate 1:1 ratio. Coupling to $^{103}$Rh was not resolved. These do not vary significantly in chemical shift or relative intensity when measured at 298 K. The observation of only two signals suggests that the disorder observed in the cation could be static (with coincident signals) or dynamic[60] (and fast[61]) on the NMR time scale, but the observation that no change is observed on changing the temperature suggests the former. $^{13}$C{$^1$H} SSNMR spectrum shows a featureless region between $\delta$ 115 and 43, indicating that the COD has been hydrogenated to COA, which is observed as a sharp signal at $\delta$ 25.7. This assignment is supported by a nonquaternary suppression experiment (NQS) which, as well as detecting quaternary carbons, identifies CH$_n$ groups that experience motion in a frequency range similar to, or greater than, the $^1$H−$^{13}$C dipolar coupling.[62,63] In the 158 K NQS spectrum a single prominent signal remains at $\delta$ 25.7 in the alkyl region, compared with the $^{13}$C{$^1$H} SSNMR spectrum (Figure 4A). This peak remains at 298 K.[39] These data

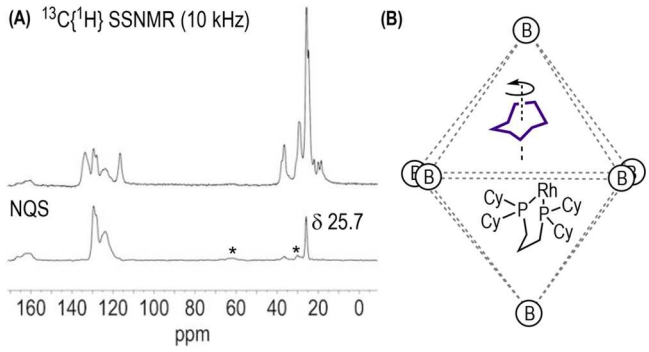


**Figure 4.** (A) $^{13}$C{$^1$H} SSNMR spectra (10 kHz, 158 K) and NQS spectra of [**2**][**COA⊂BAr$^F_4$**] (10 kHz, 158 K). * = spinning sideband. (B) Proposed fluxional processes (Ⓑ = [BAr$^F_4$]).

are consistent with the encapsulated COA undergoing a low-energy site-exchange within the cavity (Figure 4B), suggested to be due to 1,2-jumps and/or exchange between the two disordered COA components.[64] To calibrate our observations, a variable temperature NQS experiment on [**1-NBA**][**BAr$^F_4$**] showed an NBA fragment undergoing motion at 298 K which is halted at 158 K, fully consistent with previous variable temperature SSNMR studies (Figure S3).[26] [**2**][**COA⊂BAr$^F_4$**] is not stable in solution. Vacuum transfer of $CD_2Cl_2$ onto solid [**2**][**COA⊂BAr$^F_4$**] and warming to 183 K resulted in a precipitate that was persistent on warming to room temperatures. ESI-MS shows this to contain multiple dimeric hydrido-chlorides.

The structural changes evident between [**2-NBA**][**BAr$^F_4$**], a $\eta^2\eta^2$ $\sigma$-alkane complex, and [**2**][**COA⊂BAr$^F_4$**], with a nonbonding alkane, can be traced back to the change in hydrocarbon, as the {ML$_2$}$^+$ fragment is the same. Consideration of the van der Waals surfaces of NBA versus COA, Figure 5, shows that the latter presents a larger steric profile for the metal center. We suggest that this, alongside possible conformational preferences for metal binding of the alkane and noncovalent F···H−C interactions in the microenvironment (see Figures S73 and S76), are drivers for the different structural motifs observed.


DOI: 10.1021/jacs.8b09364
J. Am. Chem. Soc. 2018, 140, 14958−14970

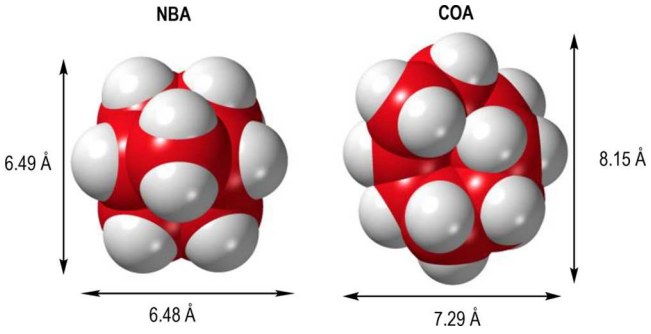


**Figure 5.** van der Waals[65] surfaces for NBA and COA.

**2.5. {Rh(Cy$_2$P(CH$_2$)$_4$PCy$_2$)}$^+$/NBA: An $\eta^2,\eta^2$-$\sigma$-Alkane Complex.** Addition of $H_2$ to single-crystals of [Rh(Cy$_2$P-(CH$_2$)$_4$PCy$_2$)(NBD)][BAr$^F_4$], [**3-NBD**][**BAr$^F_4$**], resulted in a fast (~5 min as measured by $^{31}$P{$^1$H} SSNMR spectroscopy) SC–SC transformation to give the corresponding $\sigma$-alkane complex [Rh(Cy$_2$P(CH$_2$)$_4$PCy$_2$)($\eta^2\eta^2$-NBA)][BAr$^F_4$], [**3-NBA**][**BAr$^F_4$**], Figure 6. The solid-state structure of

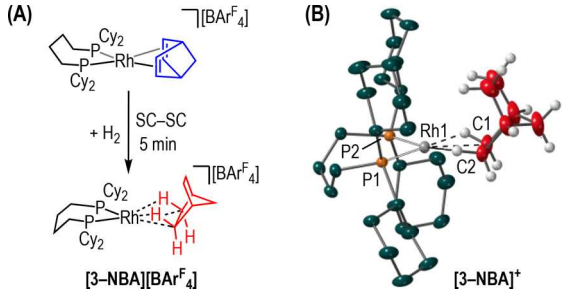


**Figure 6.** (A) SMOM synthesis of [**3-NBA**][**BAr$^F_4$**]. (B) Cation of [**3-NBA**][**BAr$^F_4$**] (50% displacement ellipsoids): Rh1···C1, 2.399(2) Å; Rh1···C2, 2.396(2) Å; Rh1–P1, 2.2154(4) Å; Rh1–P2, 2.2215(4) Å; P1–Rh1–P2, 97.87(2)°.

[**3-NBA**][**BAr$^F_4$**] reveals a $\sigma$-bound NBA ligand, with two Rh···H–C interactions using the *endo* C–H bonds (H atoms located). Despite the bite-angle increasing further compared with those of [**1-NBA**][**BAr$^F_4$**] and [**2-NBA**][**BAr$^F_4$**], the key metrics associated with this interaction remain essentially unchanged: Rh1–C1, 2.399(2) Å; Rh1–C2, 2.396(2) Å. $^{31}$P{$^1$H}, $^{13}$C{$^1$H} SSNMR and $^1$H/$^{13}$C FLSG HETCOR data (Figures S33–S36) are fully consistent with the solid-state structure, i.e., $^{31}$P{$^1$H} $\delta$ 66.7 [$J$(RhP) = 201 Hz], 49.4 [$J$(RhP) = 196 Hz]. Dissolution of [**3-NBA**][**BAr$^F_4$**] in $CD_2Cl_2$ resulted in a yellow precipitate, identified by ESI-MS, again, as a mixture of dimeric hydrido/chlorides.

Increasing the bite-angle of the phosphine promoted different *reactivity* in the resulting $\sigma$-alkane complex. Surprisingly given that the structural metrics have not changed significantly from the smaller bite-angle congeners, [**3-NBA**][**BAr$^F_4$**] is not stable when exposed to a moderate vacuum for 3 days. Crystallinity is lost, and SSNMR spectroscopy shows the formation of multiple species, as yet unidentified. Thus, although the binding of the NBA ligand appears to not be influenced significantly by the increase in bite-angle of the chelating phosphine, in the measured ground-state structure steric pressure and/or enhanced stability of any decomposition products as driven by the change in phosphine appear to promote reactivity toward loss of NBA. Hydrogenation of single-crystals of [**3-COD**][**BAr$^F_4$**] in a solid/gas reaction resulted in loss of crystallinity.[39] We have not characterized the product of this further.

**2.6. {Rh(Cy$_2$P(CH$_2$)$_5$PCy$_2$)}$^+$/COA and NBA: Phosphine Ligand Backbone C–H Activation, Structural Reorganization with Retention of Crystallinity, and Rh(III) $\eta^1$-$\sigma$-Alkane Complexes.** Addition of $H_2$ to crystalline [**4-NBD**][**BAr$^F_4$**] resulted in a rapid (~5 min as measured by $^{31}$P{$^1$H} SSNMR spectroscopy) SC–SC reaction. Analysis of the product formed using single-crystal X-ray diffraction was hampered by long-range disorder, which is also present in the starting material. The structure was modeled using a supercell ($Z'$ = 2) which gave a satisfactory solution ($R$ = 15.7%) that allowed for the gross structure of the cation to be determined, Figure 7, but does not allow for detailed metrics to be discussed.

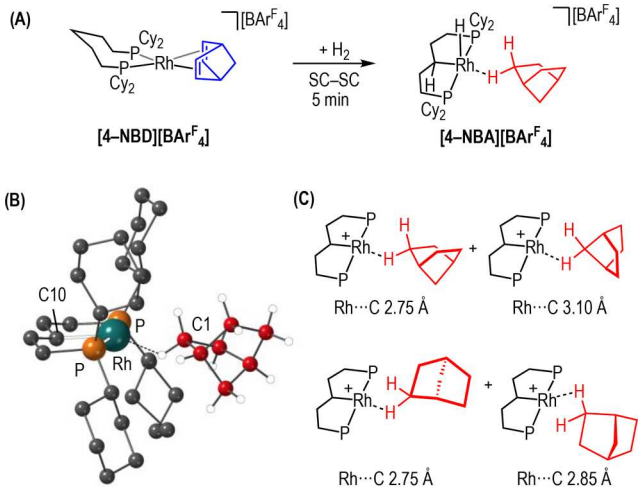


**Figure 7.** (A) Synthesis of [**4-NBA**][**BAr$^F_4$**]. (B) Ball and stick representation of one of the crystallographically independent cations in the solid-state showing one disordered NBA component, Rh–C10, ~ 2.04 Å; P–Rh–P, ~167°. (C) Representation of the four disordered NBA fragments at the two crystallographically independent cations with Rh···C(alkane) distances. Hydride positions were not determined, Cy groups not shown.

Hydrogen atoms were not located, and the NBA fragments formed by hydrogenation were necessarily modeled as rigid bodies. There are two chemically very similar, but crystallographically independent, cations in this supercell in which each has a disordered NBA over two conformations (Figure 7C). There is no crystallographically imposed local symmetry. The $O_h$ arrangement of anions in relation to each cation is retained (Figures S83–S86).

Despite the challenges associated with structural identification, it is immediately apparent that the phosphine pentamethylene backbone has undergone a C–H activation in the solid-state to form a wide bite-angle *trans*-spanning phosphine PCP pincer complex. Such intramolecular C–H activation with an R$_2$P(CH$_2$)$_5$PR$_2$ ligand has precedent in solution studies, either to form a hydrido–alkyl complex[66–68] or through a further $\alpha$-elimination to give a diphosphino-carbene complex.[69] Solution trapping experiments (*vide infra*) show that the former has occurred in [**4-NBA**]$^+$, and thus, a formulation of [Rh(Cy$_2$P(CH$_2$)$_2$(CH)(CH$_2$)$_2$PCy$_2$)H($\eta$-NBA)][BAr$^F_4$], [**4-NBA**][**BAr$^F_4$**] is proposed. The disordered NBA ligand shows a range of Rh···C distances to the Rh(III) center [2.75–3.10 Å] and interacts via either the basal or bridge methylene groups.



DOI: 10.1021/jacs.8b09364
J. Am. Chem. Soc. 2018, 140, 14958–14970

These distances reflect weak (at best) $\sigma$-interactions compared to, e.g., [**2-NBA**][**BAr$^F_4$**],[49] while this spread suggests that the NBA fragment finds a better spatial fit with the {RhPCP}$^+$ fragment for some conformations over others. The data, clearly, do not allow the precise binding mode of the alkane ($\eta^1$-HC, $\eta^3$-H$_2$C[70]) to be determined. A related SC−SC N−C oxidative addition at a Rh(I) center has been reported in Rh−PNP pincer complexes.[71] [**4-NBA**][**BAr$^F_4$**] is stable indefinitely in an Ar-filled glovebox or under vacuum.

The 298 K $^{13}$C{$^1$H} SSNMR spectrum of [**4-NBA**][**BAr$^F_4$**] shows a featureless region between $\delta$ 116 and 59, demonstrating hydrogenation of the diene. The 298 K $^{31}$P{$^1$H} SSNMR shows a tightly coupled ABX system,[72] which is less well-resolved at 158 K, consistent with inequivalent *trans*-phosphines that are in chemically very similar environments bound to a Rh(III) center: $\delta$ 64.1, 63.4 [$J$(RhP) = ∼105, $J$(PP) = 325 Hz] (Figures S49 and S50). The $^{13}$C NQS spectrum at 158 K shows at least four signals grouped between $\delta$ 38−35 and $\delta$ 29−27, in the region associated with aliphatic C−H groups, that indicate a low-energy molecular motion of the NBA ligand within the cavity of the cage (Figure S54). Such a low-energy process is consistent with the disorder of the NBA fragment modeled in the solid-state. In the 158 K FSLG HETCOR spectrum, cross peaks between these aliphatic signals in the $^{13}$C SSNMR spectrum and low-field peaks in the $^1$H projection ($\delta$ −1.8 to −2.6) are observed. We assign these to the Rh···H−C interactions, although we cannot discount ring-current effects from the proximal Ar$^F$ groups causing such a high-field shift in other C−H bonds.[18,26]

Unlike for [**2-NBA**][**BAr$^F_4$**] or [**3-NBA**][**BAr$^F_4$**], dissolving [**4-NBA**][**BAr$^F_4$**] in $CD_2Cl_2$ gave a stable complex that could be characterized by solution NMR spectroscopy and single-crystal X-ray diffraction (crystals grown from $CH_2Cl_2$/pentane) as [Rh(Cy$_2$P(CH$_2$)$_2$(CH)(CH$_2$)$_2$PCy$_2$)H($\kappa^1$-ClCH$_2$Cl)][BAr$^F_4$], [**4-CH$_2$Cl$_2$**][**BAr$^F_4$**], Figure 8, in which the NBA ligand has been

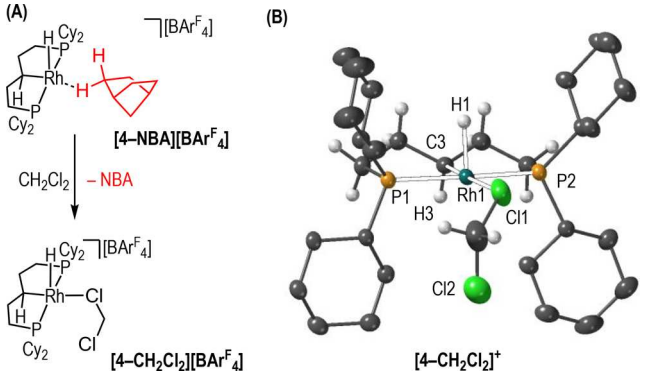


**Figure 8.** (A) Synthesis of [**4-CH$_2$Cl$_2$**][**BAr$^F_4$**]. (B) Cation of [**4-CH$_2$Cl$_2$**][**BAr$^F_4$**] (50% displacement ellipsoids): Rh1−C3, 2.074(2) Å; Rh1−P1, 2.3182(5) Å; Rh1−P2, 2.3099(5) Å; Rh1−Cl1, 2.6032(5) Å; Rh1−H1, 1.65(4) Å; P1−Rh1−P2, 167.04(2)°.

replaced by a $CH_2Cl_2$ ligand. Vacuum transfer of the volatiles demonstrates NBA is liberated, consistent with the initial solid/gas hydrogenation of the NBD to form [**4-NBA**][**BAr$^F_4$**]. The molecular structure of [**4-CH$_2$Cl$_2$**][**BAr$^F_4$**], Figure 8B, does not suffer from disorder and clearly shows the *trans*-spanning PCP pincer motif suggested for [**4-NBA**][**BAr$^F_4$**]. The Rh−hydride (H1) was located, sitting *trans* to a vacant site, and *anti* to the remaining hydrogen associated with the C−H activated methylene group (H3). This stereochemistry is as expected for an intramolecular C−H activation.[66,68] A $CH_2Cl_2$ molecule has displaced the labile NBA fragment. Displacement of a weakly bound $\sigma$-alkane ligand by halogenated solvent is well-established,[18,28,30] and the structure is consistent with other crystallographically characterized Rh−ClCH$_2$Cl complexes.[49,73,74] [**4-CH$_2$Cl$_2$**][**BAr$^F_4$**] is a 16-electron Rh(III) complex, but there is no evidence for any significant supporting agostic interaction from the cyclohexyl groups: closest Rh···C = 3.261(3) Å. Although this is not an SC−SC transformation, the $O_h$ arrangement of anions is retained in the extended solid-state structure of recrystallized material.

Solution NMR data for [**4-CH$_2$Cl$_2$**][**BAr$^F_4$**] at 298 K ($CD_2Cl_2$) reveal that a fluxional process is occurring. In the $^1$H NMR spectrum relatively broad signals are observed for the phosphine ligand, and no characteristic signal due to the C−H activated methylene (ca. 3 ppm[68]) or Rh−H was observed. The $^{31}$P{$^1$H} NMR spectrum showed a relatively sharp doublet at $\delta$ 66 [$J$(RhP) 121 Hz]. Cooling to 243 K results in a sharpening of the aliphatic region in the $^1$H NMR spectrum, and two new signals at $\delta$ 2.71 and −27.2 [d, $J$(RhH) = 55 Hz, br, fwhm ∼40 Hz] appear which integrate to 1 H each. These are assigned to the C−H activated methylene (i.e., C3) and Rh−H, respectively, the latter with a chemical shift that places it *trans* to a vacant site.[66,75,76] A spin-saturation experiment at this temperature shows that these two signals are undergoing slow mutual exchange. The $^{31}$P{$^1$H} NMR spectrum is still a doublet but is shifted slightly to lower field [$\delta$ 64.4]. These low-temperature data are fully consistent with the solid-state structure of [**4-CH$_2$Cl$_2$**][**BAr$^F_4$**]. An exchange process that involves reversible reductive C−H bond forming/C−H oxidative addition is proposed, as suggested for closely related systems,[66] and DFT calculations confirm this is favored ($\Delta G^{\ddagger}_{calc}$ = 18.7 kcal/mol) over an alternative $\alpha$−elimination process via a diphosphino−carbene intermediate ($\Delta G^{\ddagger}_{calc}$ = 27.4 kcal/mol, see Figure S105, Supporting Information).[69] It is also likely that the bound $CH_2Cl_2$ molecule is undergoing rapid exchange at the metal center with the solvent.[77]

If [**4-COD**][**BAr$^F_4$**] is subjected to $H_2$ in the solid-state, after 30 min crystallinity is lost. However, if the reaction is stopped after only 10 min and the resulting single crystals are quickly transferred to an X-ray diffractometer and cooled to 150 K, the resulting analysis shows that a new complex is formed in 30% yield in a SC−SC process, with the remainder being unreacted [**4-COD**][**BAr$^F_4$**]. These data showed this new complex to be [**4-COA**][**BAr$^F_4$**], [Rh(Cy$_2$P(CH$_2$)$_2$(CH)(CH$_2$)$_2$PCy$_2$)H($\eta^1$-COA)][BAr$^F_4$]. Although the single-crystal refinement showed a superpositional mixture of [**4-COD**][**BAr$^F_4$**] (70%) and [**4-COA**][**BAr$^F_4$**] (30%) in the $O_h$-anionic cage, refinement of the constituent components gave a reliable and robust solution ($R$ = 9.6%).

The molecular cation of [**4-COA**]$^+$ is shown in Figure 9. This shows a C−H activated, *trans*-spanning, diphosphine "PCP" pincer ligand with a cyclooctane located in close proximity to the Rh(III) metal center [Rh1a···C1a, 2.90(3) Å]. The COA ligand is not disordered and shows that all the C−C bonds are single [1.46(2)−1.48(2) Å]. The Rh···C distance is very long compared with other Rh···H−C $\sigma$-alkane complexes, cf. [**1-pentane**][**BAr$^F_4$**], 2.522(5) Å, in which the pentane acts as a bidentate ligand.[78] However, it is considerably shorter than found in [**2**][**COA⊂BAr$^F_4$**] (where we propose a minimal interaction at best) and is of a similar distance to the weak agostic interaction in *trans*-[Rh(2,2′-biphenyl)(P$^i$Bu$_3$)$_2$][BAr$^F_4$] [2.979(4) Å], as


DOI: 10.1021/jacs.8b09364
J. Am. Chem. Soc. 2018, 140, 14958−14970

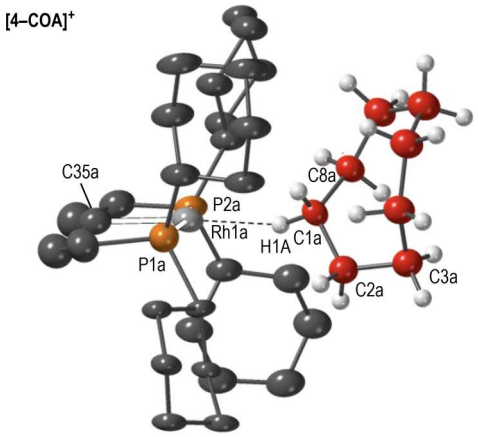


**Figure 9.** Cation of [**4-COA**][**BAr$^F_4$**] (30% displacement ellipsoids), H atoms not located, disordered [**4-COD**][**BAr$^F_4$**] not shown: Rh1a···C1a, 2.90(3) Å; Rh1−C35a, 2.08(3) Å, C1a−C2a, 1.477(2) Å; C1a−C8a, 1.45(2) Å; P1a−Rh1a−P2a, 168.5(3)°; C35a−Rh1a···C1a, 174.6(9)°; Rh1a−H1A−C1a, 140.7(2)°.

also interrogated by QTAIM analysis.[49] This distance, combined with a rather open Rh1a−H1A−C1a (albeit with the H placed in a calculated position) of 140.7(2)°, points to an $\eta^1$ Rh···H−C interaction. The hydrogen atoms were not located in [**4-COA**]$^+$, but as dissolution of the crystalline material in $CD_2Cl_2$ formed [**4-CD$_2$Cl$_2$**][**BAr$^F_4$**]/free COA alongside [**4-COD**][**BAr$^F_4$**] in a 30:70 ratio, Scheme 4, the same Rh−H,

**Scheme 4. Synthesis of [4-COA][BAr$^F_4$]**

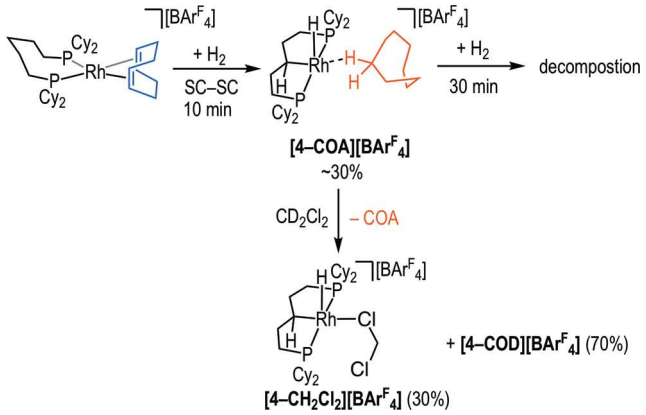


C−H activated motif as for [**4-NBA**][**BAr$^F_4$**] is proposed. As for the other $\sigma$-alkane structures reported here, there are multiple stabilizing C−H···F interactions between the alkane and proximal $CF_3$ groups in the lattice (Figure S91).

Complex [**4-COA**][**BAr$^F_4$**] is a $\sigma$-alkane complex in which only one Rh···H−C interaction is present, being related to structures characterized using solution and DFT techniques, such as [Re($\eta^6$-$C_6Me_6$)(CO)$_2$($C_5H_{10}$)][Al(OR$^f$)$_4$][31] or Rh($\eta^5$-$C_5H_5$)(CO)($C_8H_{16}$)],[79] respectively. However, as far as we are aware this is the first structurally determined example of an alkane interacting $\eta^1$ with a transition metal center. Such motifs have been probed on the picosecond time scale using fast time-resolved infrared spectroscopy (TRIR) combined with DFT calculations, and these are early intermediates in the oxidative addition of alkanes to coordinatively unsaturated metal centers.[80−82] Valence isoelectronic amine−borane and silane complexes with $\eta^1$-M···H−E coordination have been reported and show comparable structural metrics to [**4-COA**][**BAr$^F_4$**], such as wide M−H−E angles and long M···E distances: [Ir(POCOP)H($\eta^1$-HSiEt$_3$)][B($C_6F_5$)$_4$], structure A,[83] (POCOP = 2,6-[OP$^t$Bu$_2$]$_2$$C_6H_3$) and [Rh($\kappa^3$-Xantphos)-(H)$_2$($\eta^1$-$H_3B$·NMe$_3$)][BAr$^F_4$], structure B,[84] in Chart 1. Of course,

**Chart 1. Examples of $\eta^1$-Coordinated $\sigma$-Complexes[a]**

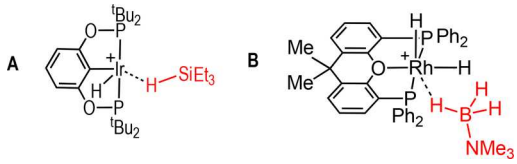


[a]Anions are not shown.

the increased polarity of the E−H bond in these analogues will make a significant contribution to bonding, and thus, they are sufficiently stable to observe using solution NMR techniques, unlike [**4-COA**][**BAr$^F_4$**].

If hydrogenation of [**4-COD**][**BAr$^F_4$**] is continued for a total of 30 min, decomposition to an, as yet unidentified, product(s) is observed upon dissolution in $CD_2Cl_2$, from which a featureless $^{31}P\{^1H\}$ NMR spectrum and a very broad $^1H$ NMR spectrum are observed. We speculate that this signals the formation of a paramagnetic Rh(II) dimeric complex on dissolution,[85] but the identity of this species remains to be resolved. Attempts to obtain meaningful SSNMR data for [**4-COA**][**BAr$^F_4$**] were hampered by temporal and temperature sensitivity that was amplified by the requirement to use finely crushed material for analysis by SSNMR that meant that crystallinity is lost much faster than for larger samples. In the $^{31}P\{^1H\}$ SSNMR spectrum at 158 K, a major, broad peak at $\delta$ 64 is observed (being similar to that seen for [**4-NBA**][**BAr$^F_4$**]), alongside [**4-COD**][**BAr$^F_4$**] and decomposition products. The sensitivity of [**4-COA**]-[**BAr$^F_4$**] contrasts with the relative stability of [**4-NBA**][**BAr$^F_4$**] or [**2**][**COA⊂BAr$^F_4$**] and perhaps reflects the combination of the different steric profile of the alkane in the former (NBA versus COA) combined with the stabilizing influence of agostic interactions in the latter.

[**4-NBA**][**BAr$^F_4$**] and [**4-COA**][**BAr$^F_4$**] are shown to have very similar structures, with the former's stability allowing for a more detailed characterization by SSNMR spectroscopy and the latter providing a good structural solution by X-ray crystallography. Combined, they thus provide a convincing analysis as a weakly bound $\sigma$-alkane complex bound $\eta^1$ at a Rh(III) center. We believe they are the first Rh(III) $\sigma$-alkane complexes isolated, or observed, by any method.

**2.7. Computational Studies.** Periodic DFT calculations were performed on the extended solid-state structures of [**X-NBA**][**BAr$^F_4$**] (X = 1,[86] 2, and 3), [**2**][**COA⊂BAr$^F_4$**], and [**4-COD**][**BAr$^F_4$**] to assess the structure and bonding of these species (see Supporting Information for details and tables of computed structures). For the [**X-NBA**][**BAr$^F_4$**] series geometries optimized with the PBE-D3 approach provided good agreement with the experimental structures. For [**2**]-[**COA⊂BAr$^F_4$**] both the major and minor components were computed and structural metrics around the Rh centers were again well-reproduced. However, more movement of the COA was seen in these calculations, perhaps reflecting the absence of significant bonded interactions between Rh and the COA (see below). For [**4-COA**][**BAr$^F_4$**] the calculations slightly underestimate the Rh1···C1 distance (calcd 2.80 Å; expt 2.90(3) Å).


DOI: 10.1021/jacs.8b09364
J. Am. Chem. Soc. 2018, 140, 14958−14970

Given the variations between computed and experimental structures across the range of systems under consideration, the subsequent analyses were based on computed structures in which the Rh, C, B, and P positions were taken from the crystallographic studies and the H and F atoms were optimized with the PBE-D3 approach. Selected distances involving key H atom positions optimized on this basis are shown in Figure 10.

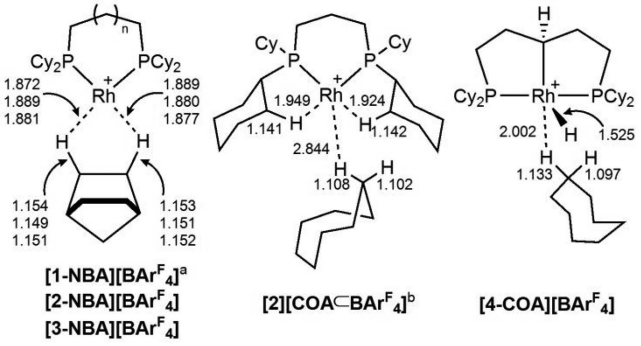


**Figure 10.** Computed distances (Å) involving key H atoms in [**X-NBA**][**BAr$^F_4$**] (X = 1, 2, and 3; *n* = 0, 1, and 2, respectively), [**2**][**COA⊂BAr$^F_4$**], and [**4-COD**][**BAr$^F_4$**]. [a]data are for *endo*-C−H bonds: all *exo*-C−H bond distances fall between 1.094 and 1.100 Å. [b]a structure based on optimization of the major component.

A more quantitative analysis of bonding was then provided by quantum theory of atoms in molecules (QTAIM) and natural bond orbital (NBO) second order perturbation donor−acceptor interaction analyses performed on the isolated cations shown in Figure 10, while noncovalent interaction (NCI) plots were run on ion pairs featuring the nearest-neighbor [BAr$^F_4$]$^-$ anion.

*2.7.1. [X-NBA][BAr$^F_4$] (X = 1, 2, and 3).* Computed structures for all three species show short Rh···H11/H21 contacts of around 1.88 Å and elongation of the C1−H11/C2-H21 bonds to *ca.* 1.15 Å consistent with the presence of two 3c−2e C−H··· Rh $\sigma$-interactions in each case. QTAIM and NBO analyses on the [**2-NBA**]$^+$ cation confirm this (Figure 11A−C), with the presence of Rh−H11 and Rh−H21 bond paths and reduced bond critical point (BCP) metrics for C1−H11 and C2−H21 compared to the spectator C1−H21/C2−H22 bonds. NBO calculations highlight the dominance of C−H → Rh $\sigma$-donation into the *trans*-$\sigma^*_{Rh-P}$ orbital, reinforced by $\pi$-back-donation from a Rh lone pair (d orbital) and the *cis*-$\sigma_{Rh-P}$ bonding orbital. Similar results were computed for [**1-NBA**]$^+$ and [**3-NBA**]$^+$ (see Supporting Information) indicating that changing the bite-angle has a minimal effect on the Rh−NBA interaction.

Figure 11D shows the NCI plot of the [**2-NBA**][**BAr$^F_4$**] ion pair and reveals a broad curved feature running roughly parallel to the H11−C1−C2−H21 bonds. This reflects the chelating nature of the NBA ligand and is predominantly stabilizing (blue) in character, while also exhibiting a central destabilizing (orange/red) region that is consistent with the presence of the ring critical point (RCP) in the QTAIM study. Some destabilizing character is also seen between Rh and the center of the two C−H bonds (see detail in Figure 11E). This suggests two cyclic {RhCH} features in the electron density topology that are consistent with an $\eta^2$-interaction and the significant contribution of classical Rh(d$\pi$) to $\sigma^*_{C-H}$ $\pi$-back-donation identified in the NBO analysis. This also highlights how the NCI approach can amplify the insight gained from the local QTAIM critical points.[87−89] These features contrast with the more

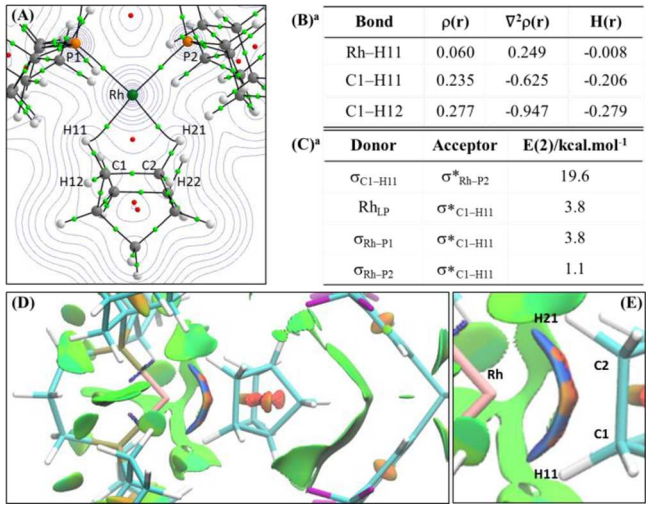


**Figure 11.** (A) Molecular graph of the [**2-NBA**]$^+$ cation; density contours plotted in the RhH11H21 plane with BCPs (green) and RCPs (red). (B) Key BCP metrics and (C) donor−acceptor interactions associated with the Rh−H11C1 interaction. (D) NCI plot of the [**2-NBA**][**BAr$^F_4$**] ion pair; isosurface generated for $s$ = 0.3 au and −0.07 < $\rho$ < 0.07 au. (E) Detail of the {Rh−NBA} interaction. [a]similar data are obtained for the Rh−H21, C2−H21, and C2−H22 interactions.

localized $\eta^1$-interactions associated with C−H···Rh bonding in [**2**][**COA⊂BAr$^F_4$**] and [**4-COA**][**BAr$^F_4$**] (see below). The NCI plot also highlights broad swathes of green that indicate weak, dispersive stabilization between the NBA ligand and (i) the aryl groups of the borate anions and (ii) the cyclohexyl substituents of the cation. Thus, intermolecular dispersion interactions play a crucial role in stabilizing these alkane ligands within the binding "pocket".[90] Similar NCI plots were obtained for [**1-NBA**][**BAr$^F_4$**] and [**3-NBA**][**BAr$^F_4$**], and a side-by-side comparison is provided in Figure S100 in the Supporting Information.

*2.7.2. [2][COA⊂BAr$^F_4$].* QTAIM and NBO data for the [**2**]$^+$ cation are displayed in Figure 12A−C. Rh−H3B and Rh−H9A bond paths signal the presence of intramolecular agostic interactions. The associated Rh···H contacts are longer (ca. 1.94 Å), and the corresponding C−H distances shorter (ca. 1.14 Å), than in the [**X-NBA**]$^+$ series, suggesting weaker interactions in [**2**]$^+$. This is confirmed by reduced $\rho(r)$ values at the Rh−H BCPs and lower $\sigma_{C-H}$ to *trans*-$\sigma^*_{Rh-P}$ $\sigma$-donation via NBO. NBO, however, also suggests a similar degree of back-donation as [**2-NBA**]$^+$, although this is not classical Rh(d$\pi$) to $\sigma^*_{C-H}$ $\pi$-back-donation but rather involves contributions from both the *cis*- and *trans*-$\sigma_{Rh-P}$ bonds (see also the discussion of [**4-COA**]$^+$ below). This suggests an $\eta^1$-C−H → Rh interaction and is supported by the NCI plot which highlights these stabilizing agostic interactions with well-defined, localized blue disks (Figure 12D,E).

The closest Rh···COA contact in [**2**][**COA⊂BAr$^F_4$**] is via H21 with a computed distance of 2.844 Å. This is well within the sum of the van der Waals radii of Rh and H (3.64 Å),[65] and a weak BCP is computed between these centers ($\rho(r)$ = 0.011 e Å$^{-3}$).[91] No equivalent donor−acceptor interaction is computed with NBO, although the NCI plot does suggest a weak, stabilizing feature between Rh and H21 (see Figure 12D,E). This is part of a broad area of weakly stabilizing interactions between the COA and the [**2**]$^+$ cation, suggesting that any direct covalent Rh···H21 interaction is at best very weak, if it exists at all. The COA is further stabilized within the cavity by dispersive interactions with the two proximate aryl substituents of the [BAr$^F_4$]$^-$ anion.[92]


DOI: 10.1021/jacs.8b09364
J. Am. Chem. Soc. 2018, 140, 14958−14970

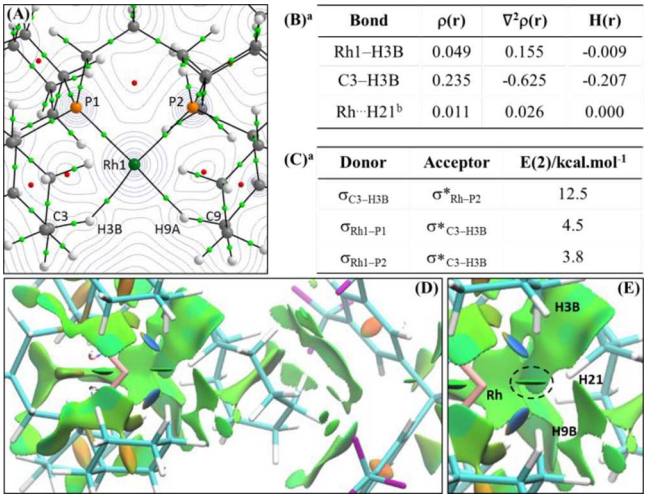


(B)[a]

| Bond | ρ(r) | ∇²ρ(r) | H(r) |
|---|---|---|---|
| Rh1–H3B | 0.049 | 0.155 | -0.009 |
| C3–H3B | 0.235 | -0.625 | -0.207 |
| Rh···H21[b] | 0.011 | 0.026 | 0.000 |

(C)[a]

| Donor | Acceptor | E(2)/kcal.mol⁻¹ |
|---|---|---|
| $\sigma_{C3-H3B}$ | $\sigma^*_{Rh-P2}$ | 12.5 |
| $\sigma_{Rh1-P1}$ | $\sigma^*_{C3-H3B}$ | 4.5 |
| $\sigma_{Rh1-P2}$ | $\sigma^*_{C3-H3B}$ | 3.8 |

**Figure 12.** (A) Molecular graph of the $[\mathbf{2}]^+$ cation; density contours plotted in the Rh(H3B)(H9A) plane with BCPs (green) and RCPs (red). (B) Key BCP metrics and (C) donor–acceptor interactions associated with the Rh–H11C1 interaction. (D) NCI plot of the $[\mathbf{2}][\mathbf{COA}\subset\mathbf{BAr^F_4}]$ ion pair; isosurface generated for $s$ = 0.3 au and $-0.07 < \rho < 0.07$ au. (E) Detail highlighting the region around Rh (the narrow disk within the circled region arises from an interaction between cyclohexyl hydrogens and sits well above the coordination plane). [a]similar data are obtained for the Rh–H9A and C9–H9A interactions. [b]COA omitted from the molecular graph for clarity, see main text and Supporting Information.

*2.7.3. [4-COA][BAr$^F_4$].* The computed structure of [**4-COA**]-[**BAr$^F_4$**] shows a Rh–H11 distance of 2.002 Å and an elongated C1–H11 distance of 1.13 Å (Figure 10). These, along with the computed Rh···H11 BCP metrics (Figure 13), suggest a

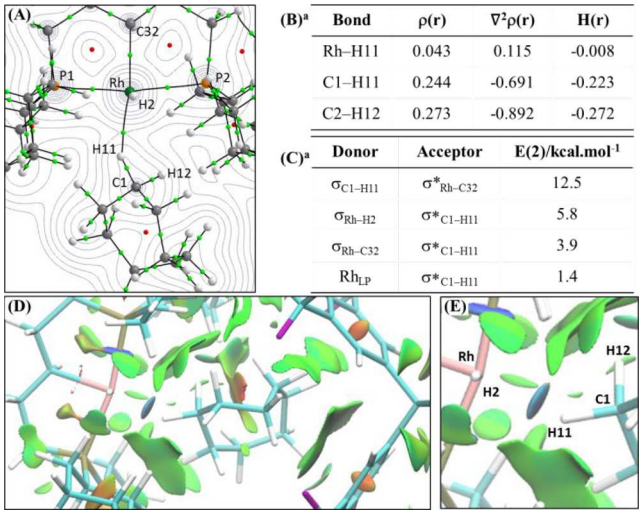


(B)[a]

| Bond | ρ(r) | ∇²ρ(r) | H(r) |
|---|---|---|---|
| Rh–H11 | 0.043 | 0.115 | -0.008 |
| C1–H11 | 0.244 | -0.691 | -0.223 |
| C2–H12 | 0.273 | -0.892 | -0.272 |

(C)[a]

| Donor | Acceptor | E(2)/kcal.mol⁻¹ |
|---|---|---|
| $\sigma_{C1-H11}$ | $\sigma^*_{Rh-C32}$ | 12.5 |
| $\sigma_{Rh-H2}$ | $\sigma^*_{C1-H11}$ | 5.8 |
| $\sigma_{Rh-C32}$ | $\sigma^*_{C1-H11}$ | 3.9 |
| $Rh_{LP}$ | $\sigma^*_{C1-H11}$ | 1.4 |

**Figure 13.** (A) Molecular graph of the $[\mathbf{4\text{-}COA}]^+$ cation; density contours plotted in the RhH11C1 plane, BCPs (green), and RCPs (red). (B) Key BCP metrics and (C) donor–acceptor interactions associated with the Rh–H11C1 interaction. (D) NCI plot of the $[\mathbf{4\text{-}COA}][\mathbf{BAr^F_4}]$ ion pair; isosurface generated for $s$ = 0.3 au and $-0.07 < \rho < 0.07$ au. (E) Detail highlighting the region around Rh.

somewhat weaker $\sigma$-interaction than in the $[\mathbf{2}]^+$ cation, although NBO indicates a similar degree of $\sigma$-donation and, if anything, greater back-donation in this case. A blue/green disk in the NCI plot confirms this $\eta^1$ C1–H11 → Rh $\sigma$-interaction as well as highlights broad areas of stabilizing dispersion interactions with the cyclohexyl substituents and the $[BAr^F_4]^-$ aryl groups.

An interesting aspect of the NBO analysis of both agostic $[\mathbf{2}]^+$ and $[\mathbf{4\text{-}COA}]^+$ is the degree of donation into $\sigma^*_{C-H}$ from the *trans*-$\sigma_{Rh-L}$ bonding orbitals (L = P2 or C32, respectively). In $[\mathbf{4\text{-}COA}]^+$, this is supported by donation from the *cis*-$\sigma_{Rh-H2}$ bonding orbital (see Figure 14). These interactions reflect the

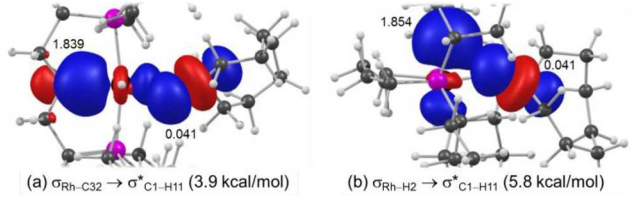


**Figure 14.** NBO donor–acceptor pairs highlighting $\sigma$-donation from (a) the *trans*-Rh–C32 $\sigma$-bond and (b) the *cis*-Rh–H2 $\sigma$-bond into $\sigma^*_{C-H}$. NBO occupancies are also indicated.

$\eta^1$-orientation of the C–H bonds in these species ($[\mathbf{2}]^+$, $\angle RhHC_{calc}(ave)$ = 138°; $[\mathbf{4\text{-}COA}]^+$, $\angle RhHC_{calc}$ = 133°). Similar $\sigma$-donation has been identified with the onset of the C–H···Rh ("pregostic") interaction[93,94] and is consistent with the end-on approach of $CH_4$ in Bürgi–Dunitz trajectories[95] and of $H_2$ in oxidative addition reactions.[96,97]

## 3. CONCLUSIONS

The studies reported herein provide a demonstration of the power of solid-state molecular organometallic chemistry (SMOM-Chem), and in particular single-crystal to single-crystal transformations to provide access to and, when combined with periodic DFT calculations, characterize a wide range of different $\sigma$-alkane M···H–C coordination motifs by systematic variation of the ligand set. Figure 15 highlights these, alongside selected

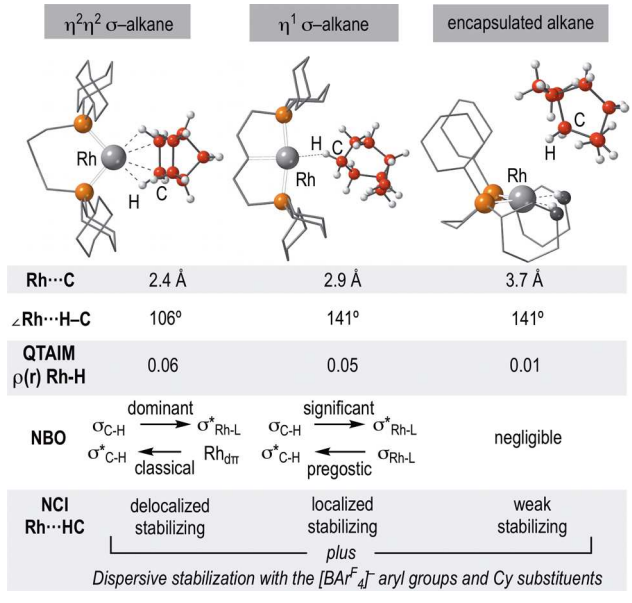


**Figure 15.** Snapshots along a continuum of M···H–C interactions provided by the complexes reported in this paper, with key, selected structural and computationally determined bonding parameters for the Rh···alkane interactions.

structural and computationally determined bonding parameters for the corresponding Rh···alkane interaction. The complexes



DOI: 10.1021/jacs.8b09364
J. Am. Chem. Soc. 2018, 140, 14958–14970

described present snapshots along a continuum of M···H−C interactions that would be very difficult to probe in σ-alkane complexes using solution techniques due to the instability of such systems combined with fluxionality between different M···H−C bonds that often results in time-averaged structures in solution, even at very low tempertaures.[14] Thus, with the NBA alkane ligand and simple, chelating phosphines, relatively strong bidentate chelating $\eta^2\eta^2$ motifs are observed, e.g., [**2-NBA**][**BAr$^F_4$**]. With a *trans*-spanning C−H activated PCP pincer ligand, reduced access to the metal center results in unprecedented $\eta^1$ Rh(III)···H−C motifs being observed in the solid-state, e.g., [**4-COA**][**BAr$^F_4$**], a model for the early stages of C−H activation at metal centers. Finally, when the steric requirement of the phosphine and the alkane combine with the ability for the phosphine to engage in stabilizing intramolecular agostic interactions, the alkane is expelled from the metal center but remarkably stays encapsulated within the anion framework, providing baseline experimental structural data for a close, but essentially nonbonding, approach of an alkane with a metal center: viz. [**2**][**COA⊂BAr$^F_4$**]. Underpinning these remarkable structures is the stabilizing effect of the anion microenvironment, and in particular the role that intermolecular dispersion interactions play in stabilizing these alkane ligands within the binding pocket. Reflecting this, none of the complexes reported are stable in solution even at low temperature. The SMOM technique thus complements elegant low-temperature *in situ* solution techniques for the synthesis and characterization of σ-alkane complexes.[29,31,81]

That such wide variations of alkane binding modes and structures are observed while a well-defined molecular environment is maintained in the solid-state provides an exemplar of a potentially tunable, molecular heterogeneous system that can be precisely characterized. By using a core metal−ligand fragment, i.e., {Rh(diphosphine)}$^+$, it also offers a wide range of potential opportunities for transformations where variation of metal−ligand interactions is likely to influence rate, stability, and selectivity in catalysis.[98] It will be interesting to see if this can be translated to productive C−H activation reactions of hydrocarbons using SMOM systems, and our efforts are currently focused in this direction.

## ■ ASSOCIATED CONTENT

### Supporting Information

The Supporting Information is available free of charge on the ACS Publications website at DOI: 10.1021/jacs.8b09364.

Synthesis, structural characterization, solution and solid-state NMR experiments, and computational studies (PDF)

Crystallographic data (CIF)

## ■ AUTHOR INFORMATION


### Corresponding Authors

*andrew.weller@chem.ox.ac.uk

*S.A.Macgregor@hw.ac.uk

### ORCID

Antonio J. Martínez-Martínez: 0000-0002-0684-1244

Bengt E. Tegner: 0000-0002-6880-9741

Alasdair I. McKay: 0000-0002-6859-172X

Simon J. Coles: 0000-0001-8414-9272

Stuart A. Macgregor: 0000-0003-3454-6776

Andrew S. Weller: 0000-0003-1646-8081


### Notes

The authors declare no competing financial interest.

## ■ ACKNOWLEDGMENTS

SCG Chemicals Co. Ltd., the EPSRC EP/M024210/1, and the Leverhulme Trust (RPG-2015-447) are acknowledged. This work used the ARCHER UK National Supercomputing Service (http://www.archer.ac.uk). We also acknowledge Professors J. Brown (Oxford) and D. Heller (Leibniz-Institut für Katalyse) for helpful discussions.

## ■ REFERENCES


(1) Hartwig, J. F. *Organotransition Metal Chemistry*; University Science Books: Sausalito, CA, 2010.

(2) van Leeuwen, P. W. N. M.; Chadwick, J. C. *Homogeneous Catalysis*; Wiley-VCH: Weinheim, 2011.

(3) van Leeuwen, P. W. N. M.; Kamer, P. C. J. Featuring Xantphos. *Catal. Sci. Technol.* **2018**, *8*, 26.

(4) Birkholz, M.-N.; Freixa, Z.; van Leeuwen, P. W. N. M. Bite angle effects of diphosphines in C-C and C-X bond forming cross coupling reactions. *Chem. Soc. Rev.* **2009**, *38*, 1099.

(5) Bilbrey, J. A.; Kazez, A. H.; Locklin, J.; Allen, W. D. Exact Ligand Solid Angles. *J. Chem. Theory Comput.* **2013**, *9*, 5734.

(6) Wilson, A. D.; Miller, A. J. M.; DuBois, D. L.; Labinger, J. A.; Bercaw, J. E. Thermodynamic Studies of $[H_2Rh(diphosphine)_2]^+$ and $[HRh(diphosphine)_2(CH_3CN)]^{2+}$ Complexes in Acetonitrile. *Inorg. Chem.* **2010**, *49*, 3918.

(7) Abdalla, J. A. B.; Caise, A.; Sindlinger, C. P.; Tirfoin, R.; Thompson, A. L.; Edwards, A. J.; Aldridge, S. Structural snapshots of concerted double E−H bond activation at a transition metal centre. *Nat. Chem.* **2017**, *9*, 1256.

(8) Corma, A. Heterogeneous Catalysis: Understanding for Designing, and Designing for Applications. *Angew. Chem., Int. Ed.* **2016**, *55*, 6112.

(9) Falkowski, J. M.; Sawano, T.; Zhang, T.; Tsun, G.; Chen, Y.; Lockard, J. V.; Lin, W. Privileged Phosphine-Based Metal−Organic Frameworks for Broad-Scope Asymmetric Catalysis. *J. Am. Chem. Soc.* **2014**, *136*, 5213.

(10) Bohnsack, A. M.; Ibarra, I. A.; Bakhmutov, V. I.; Lynch, V. M.; Humphrey, S. M. Rational Design of Porous Coordination Polymers Based on Bis(phosphine)$MCl_2$ Complexes That Exhibit High-Temperature $H_2$ Sorption and Chemical Reactivity. *J. Am. Chem. Soc.* **2013**, *135*, 16038.

(11) González-Gálvez, D.; Nolis, P.; Philippot, K.; Chaudret, B.; van Leeuwen, P. W. N. M. Phosphine-Stabilized Ruthenium Nanoparticles: The Effect of the Nature of the Ligand in Catalysis. *ACS Catal.* **2012**, *2*, 317.

(12) Thomas, J. M.; Raja, R. Exploiting Nanospace for Asymmetric Catalysis: Confinement of Immobilized, Single-Site Chiral Catalysts Enhances Enantioselectivity. *Acc. Chem. Res.* **2008**, *41*, 708.

(13) Copéret, C.; Comas-Vives, A.; Conley, M. P.; Estes, D. P.; Fedorov, A.; Mougel, V.; Nagae, H.; Núñez-Zarur, F.; Zhizhko, P. A. Surface Organometallic and Coordination Chemistry toward Single-Site Heterogeneous Catalysts: Strategies, Methods, Structures, and Activities. *Chem. Rev.* **2016**, *116*, 323.

(14) Weller, A. S.; Chadwick, F. M.; McKay, A. I. Transition Metal Alkane-Sigma Complexes: Synthesis, Characterization, and Reactivity. *Adv. Organomet. Chem.* **2016**, *66*, 223.

(15) Hall, C.; Perutz, R. N. Transition Metal Alkane Complexes. *Chem. Rev.* **1996**, *96*, 3125.

(16) Young, R. D. Characterisation of Alkane σ-Complexes. *Chem. - Eur. J.* **2014**, *20*, 12704.

(17) Pike, S. D.; Thompson, A. L.; Algarra, A. G.; Apperley, D. C.; Macgregor, S. A.; Weller, A. S. Synthesis and Characterization of a Rhodium(I) σ-Alkane Complex in the Solid State. *Science* **2012**, *337*, 1648.

(18) Pike, S. D.; Chadwick, F. M.; Rees, N. H.; Scott, M. P.; Weller, A. S.; Krämer, T.; Macgregor, S. A. Solid-State Synthesis and Character-




DOI: 10.1021/jacs.8b09364
J. Am. Chem. Soc. 2018, 140, 14958−14970

ization of σ-Alkane Complexes, $[Rh(L_2)(\eta^2,\eta^2\text{-}C_7H_{12})][BAr^F{}_4]$ ($L_2$ = Bidentate Chelating Phosphine). *J. Am. Chem. Soc.* **2015**, *137*, 820.
(19) McKay, A. I.; Krämer, T.; Rees, N. H.; Thompson, A. L.; Christensen, K. E.; Macgregor, S. A.; Weller, A. S. Formation of a σ-alkane Complex and a Molecular Rearrangement in the Solid-State: $[Rh(Cyp_2PCH_2CH_2PCyp_2)(\eta^2:\eta^2\text{-}C_7H_{12})][BAr^F{}_4]$. *Organometallics* **2017**, *36*, 22.
(20) McKay, A. I.; Martínez-Martínez, A. J.; Griffiths, H. J.; Rees, N. H.; Waters, J. B.; Weller, A. S.; Krämer, T.; Macgregor, S. A. Controlling Structure and Reactivity in Cationic Solid-State Molecular Organometallic Systems Using Anion Templating. *Organometallics* **2018**, in press. DOI: 10.1021/acs.organomet.8b00215.
(21) Kubas, G. J. *Metal Dihydrogen and σ-Bond Complexes*; Kluwer: New York, 2001.
(22) Green, J. C.; Green, M. L. H.; Parkin, G. The occurrence and representation of three-centre two-electron bonds in covalent inorganic compounds. *Chem. Commun.* **2012**, *48*, 11481.
(23) Bergman, R. G. Organometallic chemistry: C-H activation. *Nature* **2007**, *446*, 391.
(24) Goldberg, K. I.; Goldman, A. S. Large-Scale Selective Functionalization of Alkanes. *Acc. Chem. Res.* **2017**, *50*, 620.
(25) *Alkane C-H Activation by Single-Site Metal Catalysis*; Perez, P. J., Ed.; Spinger: Dordrecht, 2012; Vol. *38*.
(26) Chadwick, F. M.; Krämer, T.; Gutmann, T.; Rees, N. H.; Thompson, A. L.; Edwards, A. J.; Buntkowsky, G.; Macgregor, S. A.; Weller, A. S. Selective C−H Activation at a Molecular Rhodium Sigma-Alkane Complex by Solid/Gas Single-Crystal to Single-Crystal H/D Exchange. *J. Am. Chem. Soc.* **2016**, *138*, 13369.
(27) Geftakis, S.; Ball, G. E. Direct observation of a transition metal alkane complex, $CpRe(CO)_2$(cyclopentane), using NMR spectroscopy. *J. Am. Chem. Soc.* **1998**, *120*, 9953.
(28) Bernskoetter, W. H.; Schauer, C. K.; Goldberg, K. I.; Brookhart, M. Characterization of a Rhodium(I) -Methane Complex in Solution. *Science* **2009**, *326*, 553.
(29) Calladine, J. A.; Duckett, S. B.; George, M. W.; Matthews, S. L.; Perutz, R. N.; Torres, O.; Vuong, K. Q. Manganese Alkane Complexes: An IR and NMR Spectroscopic Investigation. *J. Am. Chem. Soc.* **2011**, *133*, 2303.
(30) Walter, M. D.; White, P. S.; Schauer, C. K.; Brookhart, M. Stability and Dynamic Processes in 16VE Iridium(III) Ethyl Hydride and Rhodium(I) σ-Ethane Complexes: Experimental and Computational Studies. *J. Am. Chem. Soc.* **2013**, *135*, 15933.
(31) Yau, H. M.; McKay, A. I.; Hesse, H.; Xu, R.; He, M.; Holt, C. E.; Ball, G. E. Observation of Cationic Transition Metal-Alkane Complexes with Moderate Stability in Hydrofluorocarbon Solution. *J. Am. Chem. Soc.* **2016**, *138*, 281.
(32) Petrosko, S. H.; Johnson, R.; White, H.; Mirkin, C. A. Nanoreactors: Small Spaces, Big Implications in Chemistry. *J. Am. Chem. Soc.* **2016**, *138*, 7443.
(33) Chadwick, F. M.; McKay, A. I.; Martinez-Martinez, A. J.; Rees, N. H.; Kramer, T.; Macgregor, S. A.; Weller, A. S. Solid-state molecular organometallic chemistry. Single-crystal to single-crystal reactivity and catalysis with light hydrocarbon substrates. *Chem. Sci.* **2017**, *8*, 6014.
(34) Thomas, J. M. *Design and Applications of Single-Site Heterogeneous Catalysts*; Imperial College Press: London, 2012.
(35) Gonzalez, M. I.; Mason, J. A.; Bloch, E. D.; Teat, S. J.; Gagnon, K. J.; Morrison, G. Y.; Queen, W. L.; Long, J. R. Structural characterization of framework-gas interactions in the metal-organic framework $Co_2$(dobdc) by in situ single-crystal X-ray diffraction. *Chem. Sci.* **2017**, *8*, 4387.
(36) Li, Z.; Peters, A. W.; Bernales, V.; Ortuño, M. A.; Schweitzer, N. M.; DeStefano, M. R.; Gallington, L. C.; Platero-Prats, A. E.; Chapman, K. W.; Cramer, C. J.; Gagliardi, L.; Hupp, J. T.; Farha, O. K. Metal−Organic Framework Supported Cobalt Catalysts for the Oxidative Dehydrogenation of Propane at Low Temperature. *ACS Cent. Sci.* **2017**, *3*, 31.
(37) Burgun, A.; Coghlan, C. J.; Huang, D. M.; Chen, W.; Horike, S.; Kitagawa, S.; Alvino, J. F.; Metha, G. F.; Sumby, C. J.; Doonan, C. J. Mapping-Out Catalytic Processes in a Metal−Organic Framework with Single-Crystal X-ray Crystallography. *Angew. Chem.* **2017**, *129*, 8532.
(38) Pike, S. D.; Crimmin, M. R.; Chaplin, A. B. Organometallic chemistry using partially fluorinated benzenes. *Chem. Commun.* **2017**, *53*, 3615.
(39) See Supporting Information.
(40) Meißner, A.; Alberico, E.; Drexler, H.-J.; Baumann, W.; Heller, D. Rhodium diphosphine complexes: a case study for catalyst activation and deactivation. *Catal. Sci. Technol.* **2014**, *4*, 3409.
(41) Heller, D.; De Vries, A. H.; De Vries, J. G. In *The Handbook of Homogeneous Hydrogenation*; Wiley-VCH: Weinheim, 2007.
(42) Green, M. L. H.; Parkin, G. In *The Chemical Bond III: 100 Years Old and Getting Stronger*; Mingos, D. M. P., Ed.; Springer International Publishing: Cham, 2017; p 206.
(43) Smart, K. A.; Grellier, M.; Coppel, Y.; Vendier, L.; Mason, S. A.; Capelli, S. C.; Albinati, A.; Montiel-Palma, V.; Muñoz-Hernández, M. A.; Sabo-Etienne, S. Nature of Si−H Interactions in a Series of Ruthenium Silazane Complexes Using Multinuclear Solid-State NMR and Neutron Diffraction. *Inorg. Chem.* **2014**, *53*, 1156.
(44) In the 298 K $^1H/^{13}C$ HETCOR, additional cross peaks are seen for signals between $\delta(^1H)$ 0 and −1 and $\delta(^{13}C)$ 17 and 20. Close inspection of the secondary interactions in [**3-NBA**][$\mathbf{BAr^F{}_4}$] reveals a number of C−H bonds in the phosphine that lie over the centers of anion aryl rings (H···C6 centroid 2.82−2.94 Å) and are thus likely to experience ring-current effects. In addition, the NBA fragment is likey undergoing a $C_2$ rotation in the solid-state on the NMR time scale at 298 K, as reported for [**1-NBA**][$\mathbf{BAr^F{}_4}$].
(45) Douglas, T. M.; Molinos, E.; Brayshaw, S. K.; Weller, A. S. Rhodium Phosphine Olefin Complexes of the Weakly Coordinating Anions $[BAr^F{}_4]^-$ and $[1\text{-closo-}CB_{11}H_6Br_6]^-$. Kinetic versus Thermodynamic Factors in Anion Coordination and Complex Reactivity. *Organometallics* **2007**, *26*, 463.
(46) Chaplin, A. B. Rhodium(I) Complexes of the Conformationally Rigid $IBioxMe_4$ Ligand: Isolation of a Stable Low-Coordinate T-Shaped Complex. *Organometallics* **2014**, *33*, 624.
(47) Ingleson, M.; Fan, H.; Pink, M.; Tomaszewski, J.; Caulton, K. G. Three-Coordinate Co(I) Provides Access to Unsaturated Dihydrido-Co(III) and Seven-Coordinate Co(V). *J. Am. Chem. Soc.* **2006**, *128*, 1804.
(48) Brookhart, M.; Green, M. L. H.; Parkin, G. Agostic interactions in transition metal compounds. *Proc. Natl. Acad. Sci. U. S. A.* **2007**, *104*, 6908.
(49) Knighton, R. C.; Emerson-King, J.; Rourke, J. P.; Ohlin, C. A.; Chaplin, A. B. Solution, Solid-State, and Computational Analysis of Agostic Interactions in a Coherent Set of Low-Coordinate Rhodium(III) and Iridium(III) Complexes. *Chem. - Eur. J.* **2018**, *24*, 4927.
(50) Sewell, L. J.; Chaplin, A. B.; Abdalla, J. A. B.; Weller, A. S. Reversible C-H activation of a $P^tBu^iBu_2$ ligand to reveal a masked 12 electron $[Rh(PR_3)_2]^+$ cation. *Dalton Trans.* **2010**, *39*, 7437.
(51) NCI plots on $[\mathbf{2}]^+$ suggest significant intramolecular dispersion stablization between the Cy groups not involved in the agostic interactions.
(52) van der Eide, E. F.; Yang, P.; Bullock, R. M. Isolation of Two Agostic Isomers of an Organometallic Cation: Different Structures and Colors. *Angew. Chem., Int. Ed.* **2013**, *52*, 10190.
(53) Meier, S. C.; Holz, A.; Kulenkampff, J.; Schmidt, A.; Kratzert, D.; Himmel, D.; Schmitz, D.; Scheidt, E.-W.; Scherer, W.; Bülow, C.; Timm, M.; Lindblad, R.; Akin, S. T.; Zamudio-Bayer, V.; von Issendorff, B.; Duncan, M. A.; Lau, J. T.; Krossing, I. Access to the Bis-benzene Cobalt(I) Sandwich Cation and its Derivatives: Synthons for a "Naked" Cobalt(I) Source? *Angew. Chem., Int. Ed.* **2018**, *57*, 9310.
(54) Douglas, T. M.; Chaplin, A. B.; Weller, A. S. Dihydrogen Loss from a 14-Electron Rhodium(III) Bis-Phosphine Dihydride To Give a Rhodium(I) Complex That Undergoes Oxidative Addition with Aryl Chlorides. *Organometallics* **2008**, *27*, 2918.
(55) Kohyama, Y.; Murase, T.; Fujita, M. Metal−Organic Proximity in a Synthetic Pocket. *J. Am. Chem. Soc.* **2014**, *136*, 2966.
(56) Ajami, D.; Rebek, J., Jr Compressed alkanes in reversible encapsulation complexes. *Nat. Chem.* **2009**, *1*, 87.


DOI: 10.1021/jacs.8b09364
J. Am. Chem. Soc. 2018, 140, 14958−14970

(57) Pakes, P. W.; Rounds, T. C.; Strauss, H. L. Conformations of cyclooctane and some related oxocanes. *J. Phys. Chem.* **1981**, *85*, 2469.
(58) Castro-Rodriguez, I.; Nakai, H.; Gantzel, P.; Zakharov, L. N.; Rheingold, A. L.; Meyer, K. Evidence for Alkane Coordination to an Electron-Rich Uranium Center. *J. Am. Chem. Soc.* **2003**, *125*, 15734.
(59) Arnold, P. L.; Prescimone, A.; Farnaby, J. H.; Mansell, S. M.; Parsons, S.; Kaltsoyannis, N. Characterizing Pressure-Induced Uranium C···H Agostic Bonds. *Angew. Chem., Int. Ed.* **2015**, *54*, 6735.
(60) Braga, D. Dynamical processes in crystalline organometallic complexes. *Chem. Rev.* **1992**, *92*, 633.
(61) Chaplin, A. B.; Green, J. C.; Weller, A. S. C−C Activation in the Solid State in an Organometallic $\sigma$-Complex. *J. Am. Chem. Soc.* **2011**, *133*, 13162.
(62) Tahir, M. I. M.; Rees, N. H.; Heyes, S. J.; Cowley, A. R.; Prout, K. Discrimination of chiral guests by chiral channels: Variable temperature studies by SXRD and solid state $^{13}$C NMR of the deoxycholic acid complexes of camphorquinone and endo-3-bromocamphor. *Chirality* **2008**, *20*, 863.
(63) Torres-Huerta, A.; Rodríguez-Molina, B.; Höpfl, H.; Garcia-Garibay, M. A. Synthesis and Solid-State Characterization of Self-Assembled Macrocyclic Molecular Rotors of Bis(dithiocarbamate) Ligands with Diorganotin(IV). *Organometallics* **2014**, *33*, 354.
(64) Lattice mobility of COA formed from solid/gas reaction between $[Ir(PPh_3)_2(COD)][PW_{12}O_{40}]$ and $D_2$ has been proposed on the basis of line shape analysis of $^2$H SSNMR spectrum. Siedle, A. R.; Newmark, R. A.; Sahyun, M. R. V.; Lyon, P. A.; Hunt, S. L.; Skarjune, R. P. Solid-state Chemistry of Molecular Metal Oxide Clusters. Multiple, Sequential C-H Activation Processes in the Hydrogenation of Coordinated Cyclooctene. Lattice Mobility of Small Organic Molecules. *J. Am. Chem. Soc.* **1989**, *111*, 8346.
(65) Alvarez, S. A cartography of the van der Waals territories. *Dalton Trans.* **2013**, *42*, 8617.
(66) Crocker, C.; Errington, R. J.; McDonald, W. S.; Odell, K. J.; Shaw, B. L.; Goodfellow, R. J. Rapid reversible fission of a C-H bond in a metal complex: X-ray crystal structure of $[RhHCl(Bu^t_2PCH_2CH_2CHCH_2CH_2PBu^t_2)]$. *J. Chem. Soc., Chem. Commun.* **1979**, 498.
(67) Brown, J. M.; Chaloner, P. A.; Kent, A. G.; Murrer, B. A.; Nicholson, P. N.; Parker, D.; Sidebottom, P. J. The mechanism of asymmetric homogeneous hydrogenation. Solvent complexes and dihydrides from rhodium diphosphine precursors. *J. Organomet. Chem.* **1981**, *216*, 263.
(68) McLoughlin, M. A.; Flesher, R. J.; Kaska, W. C.; Mayer, H. A. Synthesis and Reactivity of $[IrH_2(^tBu_2P)CH_2CH_2CHCH_2CH_2P(^tBu_2)]$, a Dynamic Iridium Polyhydride Complex. *Organometallics* **1994**, *13*, 3816.
(69) Empsall, H. D.; Hyde, E. M.; Markham, R.; McDonald, W. S.; Norton, M. C.; Shaw, B. L.; Weeks, B. Synthesis and X-ray structure of an unusual iridium ylide or carbene complex. *J. Chem. Soc., Chem. Commun.* **1977**, 589.
(70) Baratta, W.; Mealli, C.; Herdtweck, E.; Ienco, A.; Mason, S. A.; Rigo, P. Nonclassical vs Classical Metal···$H_3$C−C Interactions: Accurate Characterization of a 14-Electron Ruthenium(II) System by Neutron Diffraction, Database Analysis, Solution Dynamics, and DFT Studies. *J. Am. Chem. Soc.* **2004**, *126*, 5549.
(71) Weng, W.; Guo, C.; Moura, C.; Yang, L.; Foxman, B. M.; Ozerov, O. V. Competitive Activation of N−C and C−H Bonds of the PNP Framework by Monovalent Rhodium and Iridium. *Organometallics* **2005**, *24*, 3487.
(72) Pregosin, P. S. *NMR in Organometallic Chemistry*; Wiley-VCH: Weinheim, 2012.
(73) Taw, F. L.; Mellows, H.; White, P. S.; Hollander, F. J.; Bergman, R. G.; Brookhart, M.; Heinekey, D. M. Synthesis and Investigation of $[Cp^*(PMe_3)Rh(H)(H_2)]^+$ and Its Partially Deuterated and Tritiated Isotopomers: Evidence for a Hydride/Dihydrogen Structure. *J. Am. Chem. Soc.* **2002**, *124*, 5100.
(74) Adams, G. M.; Chadwick, F. M.; Pike, S. D.; Weller, A. S. A $CH_2Cl_2$ complex of a $[Rh(pincer)]^+$ cation. *Dalton Trans.* **2015**, *44*, 6340.
(75) Scott, N. M.; Dorta, R.; Stevens, E. D.; Correa, A.; Cavallo, L.; Nolan, S. P. Interaction of a Bulky N-Heterocyclic Carbene Ligand with Rh(I) and Ir(I). Double C−H Activation and Isolation of Bare 14-Electron Rh(III) and Ir(III) Complexes. *J. Am. Chem. Soc.* **2005**, *127*, 3516.
(76) Häller, L. J. L.; Mas-Marzá, E.; Cybulski, M. K.; Sanguramath, R. A.; Macgregor, S. A.; Mahon, M. F.; Raynaud, C.; Russell, C. A.; Whittlesey, M. K. Computation provides chemical insight into the diverse hydride NMR chemical shifts of $[Ru(NHC)_4(L)H]^{0/+}$ species (NHC = N-heterocyclic carbene; L = vacant, $H_2$, $N_2$, CO, MeCN, $O_2$, $P_4$, $SO_2$, $H^-$, $F^-$ and $Cl^-$) and their $[Ru(R_2PCH_2CH_2PR_2)_2(L)H]^+$ congeners. *Dalton Trans.* **2017**, *46*, 2861.
(77) Huang, D.; Huffman, J. C.; Bollinger, J. C.; Eisenstein, O.; Caulton, K. G. The First $\eta^2$-$CH_2Cl_2$ Adduct of Ru(II):$[RuH(\eta^2$-$CH_2Cl_2)(CO)(P^tBu_2Me)_2][BAr'_4]$ (Ar′ = 3,5-$C_6H_3(CF_3)_2$) and Its $RuH(CO)(P^tBu_2Me)_2^+$ Precursor. *J. Am. Chem. Soc.* **1997**, *119*, 7398.
(78) Chadwick, F. M.; Rees, N. H.; Weller, A. S.; Krämer, T.; Iannuzzi, M.; Macgregor, S. A. A Rhodium−Pentane Sigma-Alkane Complex: Characterization in the Solid State by Experimental and Computational Techniques. *Angew. Chem.* **2016**, *128*, 3741.
(79) Pitts, A. L.; Wriglesworth, A.; Sun, X.-Z.; Calladine, J. A.; Zarić, S. D.; George, M. W.; Hall, M. B. Carbon−Hydrogen Activation of Cycloalkanes by Cyclopentadienylcarbonylrhodium—A Lifetime Enigma. *J. Am. Chem. Soc.* **2014**, *136*, 8614.
(80) Guan, J.; Wriglesworth, A.; Sun, X. Z.; Brothers, E. N.; Zarić, S. D.; Evans, M. E.; Jones, W. D.; Towrie, M.; Hall, M. B.; George, M. W. Probing the Carbon−Hydrogen Activation of Alkanes Following Photolysis of Tp'Rh(CNR)(carbodiimide): A Computational and Time-Resolved Infrared Spectroscopic Study. *J. Am. Chem. Soc.* **2018**, *140*, 1842.
(81) Asplund, M. C.; Snee, P. T.; Yeston, J. S.; Wilkens, M. J.; Payne, C. K.; Yang, H.; Kotz, K. T.; Frei, H.; Bergman, R. G.; Harris, C. B. Ultrafast UV Pump/IR Probe Studies of C−H Activation in Linear, Cyclic, and Aryl Hydrocarbons. *J. Am. Chem. Soc.* **2002**, *124*, 10605.
(82) Balcells, D.; Clot, E.; Eisenstein, O. C—H Bond Activation in Transition Metal Species from a Computational Perspective. *Chem. Rev.* **2010**, *110*, 749.
(83) Yang, J.; White, P. S.; Schauer, C. K.; Brookhart, M. Structural and Spectroscopic Characterization of an Unprecedented Cationic Transition-Metal $\eta^1$-Silane Complex. *Angew. Chem., Int. Ed.* **2008**, *47*, 4141.
(84) Johnson, H. C.; McMullin, C. L.; Pike, S. D.; Macgregor, S. A.; Weller, A. S. Dehydrogenative Boron Homocoupling of an Amine-Borane. *Angew. Chem., Int. Ed.* **2013**, *52*, 9776.
(85) Zhu, D.; Sharma, A. Z.; Wiebe, C. R.; Budzelaar, P. H. M. Rhodium(II) dimers without metal-metal bonds. *Dalton Trans.* **2015**, *44*, 13460.
(86) A previous study on [**1-NBA**][$\mathbf{BAr^F_4}$] used a slightly different protocol (ref 18), and so, this system was recomputed with the current approach for consistency. Data that are very similar to those of our previous study were obtained.
(87) Contreras-García, J.; Johnson, E. R.; Keinan, S.; Chaudret, R.; Piquemal, J.-P.; Beratan, D. N.; Yang, W. NCIPLOT: A Program for Plotting Noncovalent Interaction Regions. *J. Chem. Theory Comput.* **2011**, *7*, 625.
(88) Narth, C.; Maroun, Z.; Boto, R. A.; Chaudret, R.; Bonnet, M.-L.; Piquemal, J.-P.; Contreras-García, J. In *Applications of Topological Methods in Molecular Chemistry*; Chauvin, R., Lepetit, C., Silvi, B., Alikhani, E., Eds.; Springer International Publishing: Cham, 2016.
(89) Lane, J. R.; Contreras-García, J.; Piquemal, J.-P.; Miller, B. J.; Kjaergaard, H. G. Are Bond Critical Points Really Critical for Hydrogen Bonding? *J. Chem. Theory Comput.* **2013**, *9*, 3263.
(90) It has been recently suggested that dispersion may also contribute to intramolecular C−H···M interactions. See: Lu, Q.; Neese, F.; Bistoni, G. Formation of Agostic Structures Driven by London Dispersion. *Angew. Chem., Int. Ed.* **2018**, *57*, 4760−4764.
(91) Additional weak Rh···H−C interactions with similar BCPs metrics were also computed involving cyclohexyl C−H bonds in [**3-NBA**]$^+$ and [**2**]$^+$. See Supporting Information.


DOI: 10.1021/jacs.8b09364
*J. Am. Chem. Soc.* 2018, 140, 14958−14970

(92) The COA sits within a square-pyramidal array of $BAr^F_4$ anions (cf. Figure 3), and Figure 13 shows the "axial" $[BAr^F_4]^-$ anion. Stabilizing noncovalent interactions are also seen for the four basal $[BAr^F_4]^-$ anions, but these are less significant (see Figure S91, Supporting Materials).
(93) Scherer, W.; Dunbar, A. C.; Barquera-Lozada, J. E.; Schmitz, D.; Eickerling, G.; Kratzert, D.; Stalke, D.; Lanza, A.; Macchi, P.; Casati, N. P. M.; Ebad-Allah, J.; Kuntscher, C. Anagostic Interactions under Pressure: Attractive or Repulsive? *Angew. Chem., Int. Ed.* **2015**, *54*, 2505.
(94) Nielson, A. J.; Harrison, J. A.; Sajjad, M. A.; Schwerdtfeger, P. Electronic and Steric Manipulation of the Preagostic Interaction in Isoquinoline Complexes of RhI. *Eur. J. Inorg. Chem.* **2017**, *2017*, 2255.
(95) Crabtree, R. H. The organometallic chemistry of alkanes. *Chem. Rev.* **1985**, *85*, 245.
(96) Macgregor, S. A.; Eisenstein, O.; Whittlesey, M. K.; Perutz, R. N. A theoretical study of $[M(PH_3)_4]$ (M = Ru or Fe), models for the highly reactive $d^8$ intermediates $[M(dmpe)_2]$ (dmpe = $Me_2PCH_2CH_2PMe_2$). Zero activation energies for addition of CO and oxidative addition of $H_2$. *J. Chem. Soc., Dalton Trans.* **1998**, 291.
(97) Similar $\sigma$-donation is also seen in $[\mathbf{2\text{-}NBA}]^+$, but this is weak (1.1 kcal/mol, from *cis*-$\sigma_{RhP2}$) reflecting the tighter computed RhHC angle (102°).
(98) *Applied Homogeneous Catalysis with Organometallic Compounds*; Cornils, B., Herrmann, W. A., Beller, M., Paciello, R., Eds.; Wiley-VCH: Weinheim, 2017.



DOI: 10.1021/jacs.8b09364
*J. Am. Chem. Soc.* 2018, 140, 14958−14970